

The Effect of Bathymetry Changes on Meridional Overturning Currents

Marte Voorneveld
5911591

June 12, 2020

Abstract

We investigate the effect of changing geometries in a simple ocean general circulation model. Using highly idealized forcings we compare the situations for every 5 Milion year (Ma) time step from 65Ma to the present day situation. The present day simulation was used as a control. The model result shows a reversal of the flow through the panama gateway in the early Miocene coinciding with the closure of the Thetys seaway. We also observe a system that is extremely sensitive to the position of the Indian Continent in the Paleocene. Furthermore we observe large differences in the thermohaline circulations in comparison to the present day situation.

1 Introduction

The geography and bathymetry (depth profile of the ocean) of our planet is an ever-changing phenomenon. In the last 120 Ma (million years), the earth moved from having one major oceanic system in the Pacific, to the current 3 ocean system (Besse and Courtillot 2002). The Bathymetry changes that occurred in this period are characterized by the opening and closing of certain passages through which exchange of water between oceanic basins is observed. These passage changes are a vital part of understanding the global thermohaline circulation. The exact timing of passage openings is a topic of rigorous debate in literature (Scher and Martin 2006, Schmidt 2007).

However, one of the changes on which there is a consensus; is the inception and expansion of the Atlantic ocean. This expansion results in a decrease in the size of the Pacific basin. The creation of the Atlantic basin has had major effects on the earth's climate, resulting in massive localized changes such as the temperate European climate. The North Atlantic meridional overturning circulation (AMOC) is now understood to be essential to the present-day thermohaline circulation. The AMOC is the result of a deep water formation in the North At-

lantic. In the northern Atlantic, there is a northward flow of water with substantial heat energy. This water sinks when it reaches the arctic waters. This is because the flow rapidly loses its heat energy due to the large temperature gradient in the arctic. The loss of energy causes an increase in density and subsequent sinking of the flow. This flow is often called the "ocean Conveyer belt", a term first coined by Broecker 1991. However, it is unknown when exactly this northern sinking started. With the past nonexistence of the Antarctic Circumpolar Current (ACC) and the relatively small size of the Atlantic ocean, the AMOC must have seen its inception sometime in the last 40Ma (Abelson and Erez 2017).

The result of these bathymetry changes on the oceanic stream function and the resulting overturning currents are something that have been previously studied by Mulder et al. 2017. However, they found that using a 3D model for different geographies in each of the model years failed to simulate the onset of the Northern sinking AMOC. They used a continuation method for the forcing of each timestep, taking the previous timestep as a reference. In this paper we propose to use a similar general ocean circulation model (GCM) with only a changing bathymetry and highly simplified zonal

forcings. To accomplish this we use the relatively young GCM Veros.

This paper will focus on the effect of changes in bathymetry when using highly simplified zonally averaged forcings for the last 65Ma. The results of the model will be used to estimate global changes in oceanic throughflow at oceanic passages. Furthermore, the strength of the meridional overturning currents (MOC) and the thermohaline circulation will be studied.

2 Methods

2.1 Veros

Veros is an ocean general circulation model (GCM) based on the successful *pyOM2* model (Hafner et al. 2018). It was designed from the ground up with flexibility in mind. This flexibility cuts valuable time spent on figuring out the often cumbersome Fortran models of the past. Veros is specifically well suited for researching the effect of changes in both forcings and bathymetries. They can be easily edited using Python. These features in particular are heavily used in this paper. One of the most extensively used attributes is the fact that any bathymetry can, without further manual specifications, be used for stream function calculation. The fact that Veros is fully written in Python is also useful as it is a far more widespread language than Fortran and it is thus much easier to teach Veros to new students.

Veros uses an Arakawa C-grid for its calculations of finite differences. Here Veros uses a separate grid for tracers (temperature, salinity and density) than the grid used for vertical fluxes (velocities). For a more specific overview of the functionality the reader is referred to the *pyOM2 documentation*.

In this case, the models used are run on an 8 core (16 threads) machine using an MPI CPU configuration of 1 node. This is sufficient for the lower resolution models used in this paper. But it is noted that Veros does allow the usage of multiple nodes to do calculations on much higher resolution problems.

2.2 Model Setup

2.2.1 Model Domain

The domain of the model is bounded by longitudes $\phi_E = -180^\circ$ and $\phi_W = -180^\circ$ and latitudes

$\theta_N = 80^\circ$ and $\theta_S = -80^\circ$ with periodic boundary conditions in the zonal direction. The depth profile has 15 layers with grid stretching (fig. 1). The grid stretching relation is such that surface layers are much shallower than deep water layers. There are 90×40 horizontal grid points to make a $4^\circ \times 4^\circ$ resolution model.

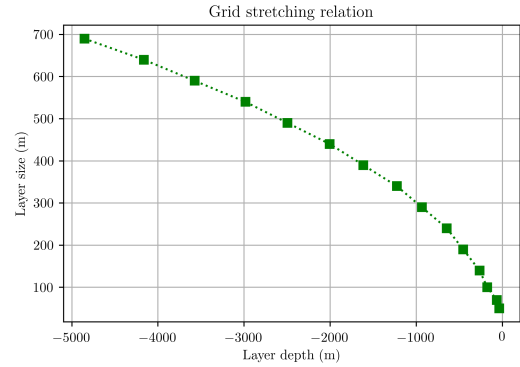


Figure 1: Grid stretching relation used for the model setup. Showing the size of the layer for each layer. Upper layers are shallower than deep water layers.

2.2.2 Surface Forcings

The Veros setup used here has restoring boundary conditions. These restore the boundary at the surface of the oceanic basin to a forcing field for Sea Surface Temperature (SST), Sea Surface Salinity (SSS), wind stress (τ) and heat flux. Choosing the correct forcing for the ocean is important. It is known that in general circulation models the MOC is sensitive to small changes in surface forcings (Milloff et al. 1999). Attempts at making these forcings highly idealized have often been made in the past with varying rates of success(Bryan 1987; Mulder et al. 2017). We note the fact that using idealized forcings will induce errors, especially in the shape of the thermohaline circulations. The use of idealized forcings is however justified here, because we are only interested in large scale features of the meridional overturning and wind-driven circulations.

Several methods were explored when making these idealized forcings. In the Mulder et al. 2017 paper an analytic forcing profile was used for wind stress, SST, and SSS (fig. 2). However, Veros is a seasonally forced model, using simplified forcings would thus fail to capture seasonal changes in the SST. There have been studies suggesting that these seasonal forcings can have large effects

on the strength of the meridional overturning circulation (Schmittner and Stocker 2001). Here we propose to take the SSS and SST profiles as zonal means of realistic forcings. We use $1^\circ \times 1^\circ$ forcings from the European Centre for Medium-Range Weather Forecasts (ECMWF) public dataset as a basis (ECMWF 2020). While the zonal wind stress is set to the simple profile proposed by Bryan 1987. The choice of this analytic profile was made over a

zonally averaged forcing mirrored along the equator ($\mu(\tau_x)$). These forcings proved to be problematic in the polar regions (fig. 2d). Both forcings were initially tested on the present-day configuration to see which most accurately captures the present-day MOC. After some initial tests, we found that $\mu(\tau_x)$ is very weak in the sub polar regions and subsequently fails to force the North Atlantic Deep Water formations (NADW).

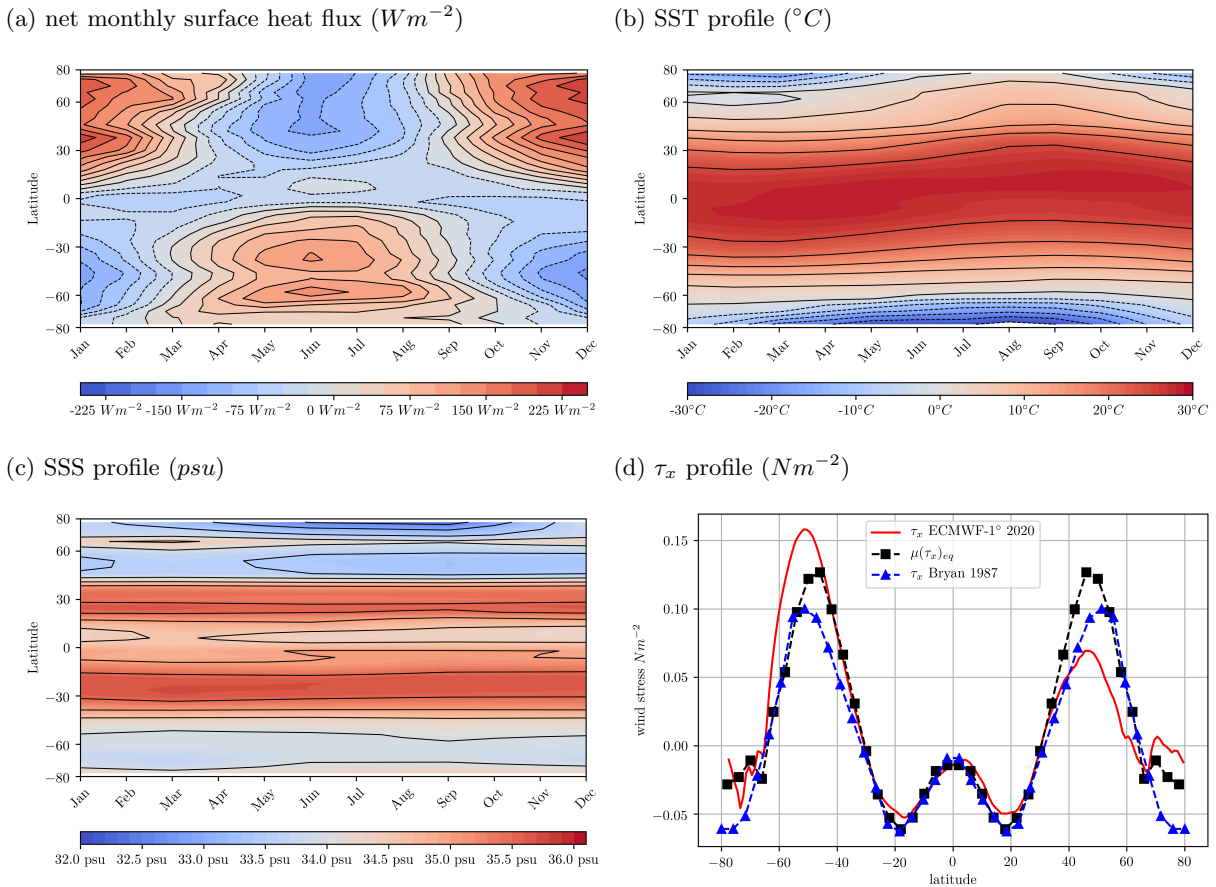


Figure 2: Zonal mean annual forcing profiles for **a)** The net monthly surface heat flux forcing profile for each latitude. Showing large annual variation in surface heat flux. **b)** The monthly Sea Surface Temperature (SST) forcing profile. Showing annual variation in the net surface temperature. **c)** Sea Surface Salinity (SSS) forcing profile showing little annual variation. **d)** The zonal wind stress profiles (τ_x) that were looked at. The red line shows the zonal average of the *ECMWF – 1°* forcings. The black squares show zonally averaged *ECMWF – 4°* forcings that were mirrored along the equator. The Blue triangles show analytic forcing profile from Bryan 1987

2.2.3 Forcing bias

The forcings used in this paper have large errors compared to the present day realistic forcings. This can be seen if we compare them to their original realistic forcings. In fig. 3 the errors compared to present-day forcings are shown. There is a large discrepancy in the Atlantic, which has a much higher salinity in the realistic forcings than in the idealized forcings. This may have implications on the thermohaline circulation we will observe in our model. It is furthermore noted that the northern Atlantic

ocean is much warmer in reality than in our model, which again possibly can affect the thermohaline circulation. Furthermore, it is also noted that the temperature on earth was also much higher in the early part of the 65Ma period (Hansen et al. 2013). We neglect this effect because we use the same forcing for each time step. Therefore, it is not possible to compare our results directly with existing proxies. However, studying the effect of geometry changes specifically is much clearer using this method and allows a deeper insight in changes induced by the geometry.

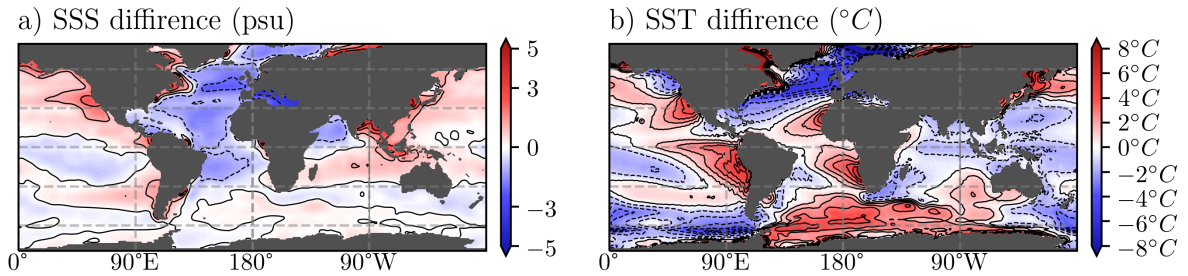


Figure 3: Errors in surface forcing. As a difference between ECMWF-1° forcings and their zonal mean. Here positive values are over estimations of the forcings. Errors for: **a)** the SSS difference with contours every 1 psu and **b)** the SST difference with contours every 1 °C

2.2.4 Initial conditions

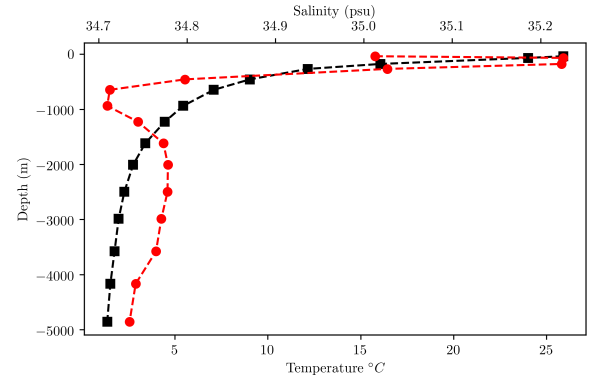


Figure 4: Temperature and salinity profiles at 2°N. Black squares indicate the Temperature (°C) profile and red circles indicate the salinity (psu) profile. Profiles from ECMWF 2020 scaled to 15 depth layers with grid stretching.

The model is started with an initial temperature and salinity profile. The profile is scaled from forcings taken from observational data (ECMWF 2020). The profiles are again use zonal means. This results in the profile seen for the situation around the equator in fig. 4.

2.2.5 MOC stream function

The global Meridional Overturning Circulation Ψ_{MOC} is defined as the zonally integrated meridional volume transport of water in the world's oceans. It can be written down as:

$$\Psi_{MOC}(y, z) = \int_z^0 \int_{180^\circ E}^{180^\circ W} v(x, y, z') dx dz'. \quad (1)$$

Here v is the meridional component of the velocity. Ψ_{MOC} is thus a stream function of the zonally integrated volume transport in the Earth's ocean basins. Plotting this stream function can give a lot of insight into the deep water transport associated with the thermohaline circulation. In this paper, we hope to capture these deepwater transport formations. In particular, we are looking for the shape of the North Atlantic deep water (NADW) and the Antarctic Bottom Water (AABW) formations (fig. 5).

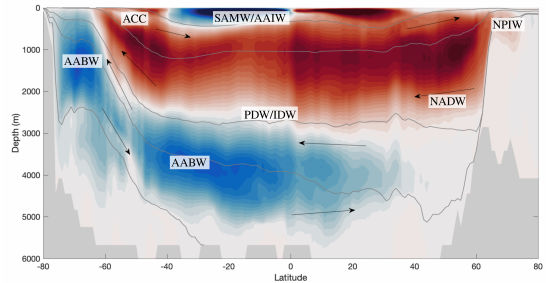


Figure 5: Meridional overturning circulation from observations taken from Forget et al. 2015. With schematic arrows indicating flow direction. Also including locations of major overturning flows. AABW: Antarctic Bottom Water, NADW: North Atlantic Deep Water, NPIW: North Pacific Intermediate Water, SAMW: Subantarctic Mode Water, AAIW: Antarctic intermediate Water, ACC: Antarctic Circumpolar Current.

2.2.6 Barotropic Stream Function

It is furthermore interesting to look at an expression for the transport of ocean gyres. We know that the depth-integrated flow must be horizontally non-divergent. Thus a stream function Ψ_b can be introduced:

$$U = -\frac{\partial \Psi_b}{\partial y}; V = \frac{\partial \Psi_b}{\partial x} \quad (2)$$

$$\Psi_b(x, y) = \int_{easternbdy}^x \int_{-D}^0 v(x', y, z) dz dx'. \quad (3)$$

Here $v(x, y, z)$ is the meridional velocity and $u(x, y, z)$ is the zonal flow. This so-called barotropic stream function (BSF) Ψ_b is defined by integrating the meridional transport westward from the eastern boundary of the domain. It is a useful tool to look at the shape and gyres associated with the major ocean current systems. By using the Sverdrup relation:

$$\int_{-D}^0 v(x, y, z) dz = \frac{1}{\beta \rho_{ref}} \vec{z} \cdot \nabla \times \tau \quad (4)$$

which was first proposed by Sverdrup 1947. We can look at a schematic diagram of the barotropic stream function based on the prevailing zonal winds (fig. 6). It is clear that the prevailing zonal winds relate to the wind stress forcing seen in fig. 2. The calculation of the barotropic stream function without easily defined boundaries is quite a bit more cumbersome than a simple integration from the eastern boundary. Veros uses a process in which special treatment is given to boundaries using something called island integrals. This is why the barotropic stream function has values below the land mask in Veros.

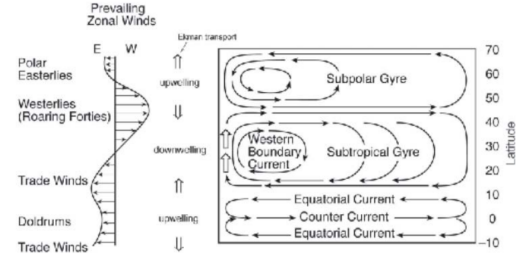


Figure 6: Schematic of the barotropic stream function based on the Sverdrup relation. Showing the subpolar and subtropical Gyres and equatorial currents. Figure taken from John Marshall 2012

2.2.7 Passage throughflow

For passages between larger oceanic basins it is interesting to look at the total transported volume of water and the direction of this flow. The location of the passages that will be studied can be seen in fig. 8. The volume transport in the zonal direction through an area A is defined as

$$Q = \iint_A u(x, y, z) dA. \quad (5)$$

Here we integrate the zonal velocity over an area A in the latitude-vertical direction that is normal to this velocity. By applying eq. (2) to eq. (5) we can thus use the output of the BSF Ψ_b to find the zonal volumetric flux through each grid cell in our model. We use the BSF output over the velocity output because the BSF is more accurate than the velocity field. This is because the velocity field is a derived quantity in veros. While the BSF is calculated every integration step.

For each passage a suitable location is chosen such that there are no boundaries next to the passageways, this is done for each time step. In fig. 7 an example of this method is shown for 20Ma. This method is the same for each of the passages

and thus we can study the effect of changes in bathymetry to on the relative strength of the flow. However, it should be noted that these values may not represent real physical values. As the passages in a 4° model are often only a few grid cells wide. Resulting in discrepancies in the calculation of the throughflow due to boundary conditions. In fig. 8 An overview is shown of all the passages discussed in this paper.

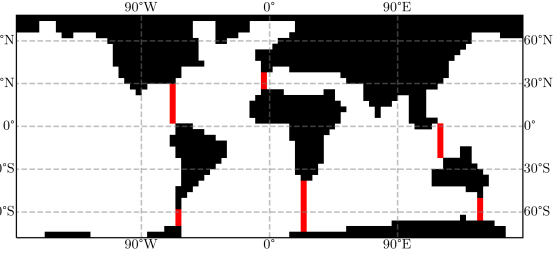


Figure 7: Example of the chosen grid cells for individual passages for 20Ma. The land mask shown here is the land mask excluding grid cells used for the BSF boundary conditions and is thus not the same as the land mask used for the model itself.

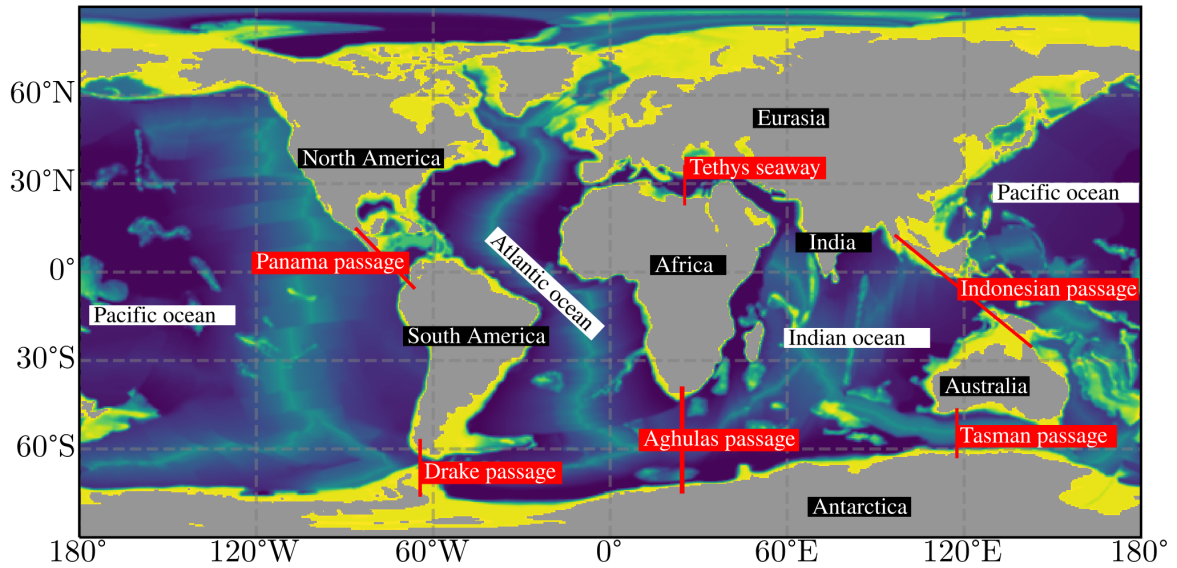


Figure 8: Schematic image showing the 30 Ma bathymetry in $0.5^\circ \times 0.5^\circ$. Overlayed in red are the passages we study. In black the continents and in white the oceanic basins.

2.3 Creating Bathymetries

To facilitate the model a set of 14 bathymetries was created in 5Ma time steps. These run from 65Ma to the present-day configuration. These were reconstructed from bathymetries gained in Baatsen et al. 2016. These bathymetries which originally were $0.5^\circ \times 0.5^\circ$ have been scaled to a $4^\circ \times 4^\circ$ model using Gaussian interpolation. Next, the land masks were manually edited to include passages and exclude some inland seas. Due to the low resolution of the model, choices have to be made concerning the opening of certain passages. One of the choices that were made is that the northern Arctic sea is closed off in all of the bathymetries. This is mainly since $4^\circ \times 4^\circ$ models do not have enough resolution to facilitate this sea and Veros lacking the ability to have polar flow. The main events that shape the oceanic passages can be divided into periods. These periods are defined in table 1.

	From	Until
Paleocene	65Ma	55Ma
Eocene	50Ma	35Ma
Oligocene	30Ma	25Ma
Miocene	20Ma	10Ma
Pliocene	5Ma	present

Table 1: Time periods covered by this paper

The discussion on each period is split into separate subsections. Here we address each of the periods and their respective changes.

2.3.1 Paleocene

In the Paleocene a vast Pacific exists almost serving as a single basin. This period is largely characterized by the growth and development of a larger atlantic basin. Subsequently a decrease in size of the pacific basin is also observed. The drake passage is explicitly chosen to be closed in this time period, there is some evidence of it being opened in the paleocene due to a major change in the motion of the South American and Antarctic plates until about 50Ma (Livermore et al. 2005). However, the evi-

dence proposes a shallow opening of less than 1 km in depth. These uncertainties and the shallow nature of the opening has led to the decision to close the passage until its certain deep water connection starting after the late Eocene as also indicated by Livermore et al. 2005.

It is also interesting to note the existence of a range of islands between the Indian continent and the Eurasian continent which disappears in this period. These islands are called the Kohistan-Ladakh Arc (Jagoutz, Bouilhol, and Upadhyay 2009). These may have had quite significant effect on the flow through the thetys seaway and are thus an interesting topic to discuss later on.

2.3.2 Eocene

The Eocene in contrast to the Paleocene is distinguished by the opening of certain passages connecting oceanic basins. These effects are often studied extensively for each individual passage in literature. Choosing the exact timing for opening the passages is done manually by looking at often active research. The first of such passages to open is the Tasman passage which is opened at 35Ma as a shallow passage slowly growing in size(Lawver and Gahagan 2003). The Tasman passage opening is believed to have had a large impact on the onset of the Atlantic circumpolar current (ACC). Some authors even suggests its influence on the onset of a early "proto-ACC" (Sarkar et al. 2019). This proto-ACC may have caused upwelling of northern-sourced nutrient-rich deep equatorial Pacific waters in the south Pacific. However, this is assuming an open drake passage, which does not exist in our bathymetries. Thus, this upwelling will likely not be observed until the early Oligocene.

From the onset of the early Eogene the Indian Continent has been fast moving towards the north slowly closing the northern passage between the Indian ocean and the Tethys seaway. The deep water passage is closed from 35Ma based onwards Najman et al. 2010. This limits the throughflow through the Thetys seaway to purely east of the Indian continent. Which is now in effect part of the larger Eurasian continent.

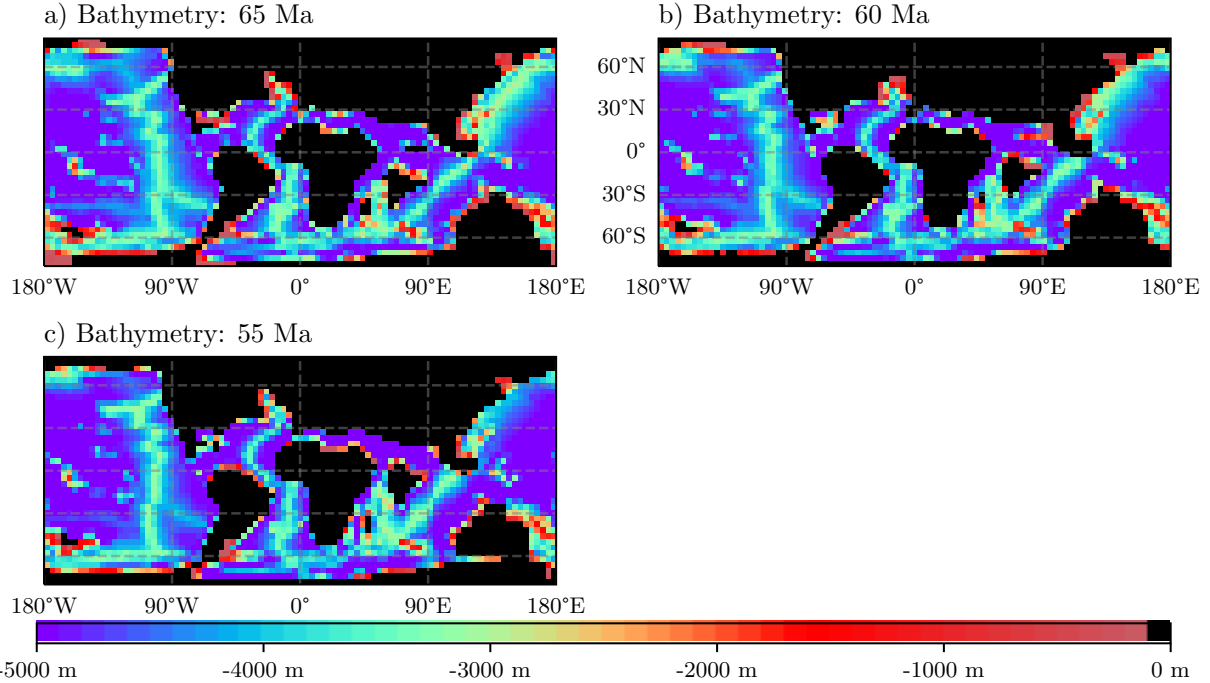


Figure 9: Paleocene bathymetries, black squares show the land mask used. The bathymetries for (a) 65 Ma including the Kohistan-Ladakh Arc (b) 60 Ma showing submergence of the Kohistan-Ladakh Arc (c) 55 Ma here the gap between Africa and South America is seen to grow.

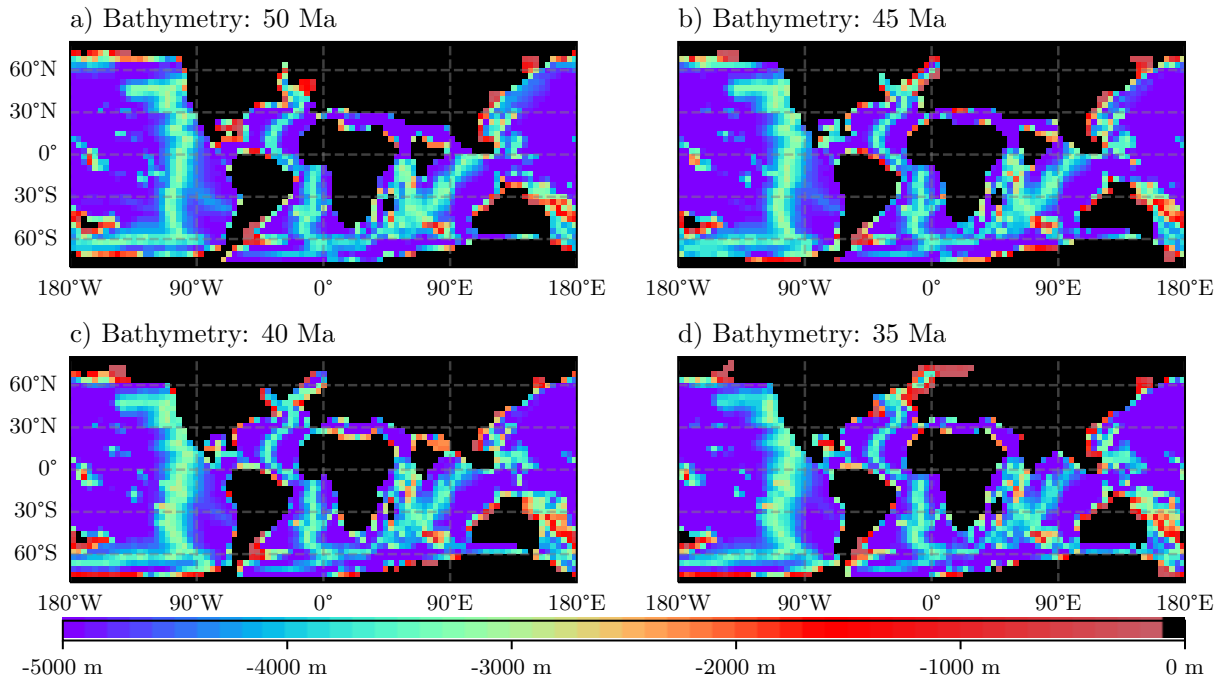


Figure 10: Eocene bathymetries, black squares show the land mask used. The bathymetries for (a) 50 Ma, (b) 45 Ma, (c) 40 Ma, (d) 35 Ma showing the opening of the Tasman Passage by the detachment of the Australian continent from Antarctica. Also, water passage over India is closed.

2.3.3 Oligocene

From the onset of the Oligocene, the total circulation of water around the Antarctic basin is finalized by the opening of the shallow Drake passage at around 30Ma. 30Ma is specifically chosen to differentiate between the opening of the drake and Tasman passages. Especially since there is still some debate on the exact timing of drake passage opening (Scher and Martin 2006; Livermore et al. 2005).

These openings coincide with the onset of the ACC that has had major effects on the global climate variability. Furthermore, The Oligocene is characterized by the further expansion of the Atlantic basin and a shallower Thetys seaway. Furthermore, a deep water area starts existing between what is now Greenland and the European continent. This water basin is now known to be central to the deep-water formations of the northern Atlantic.

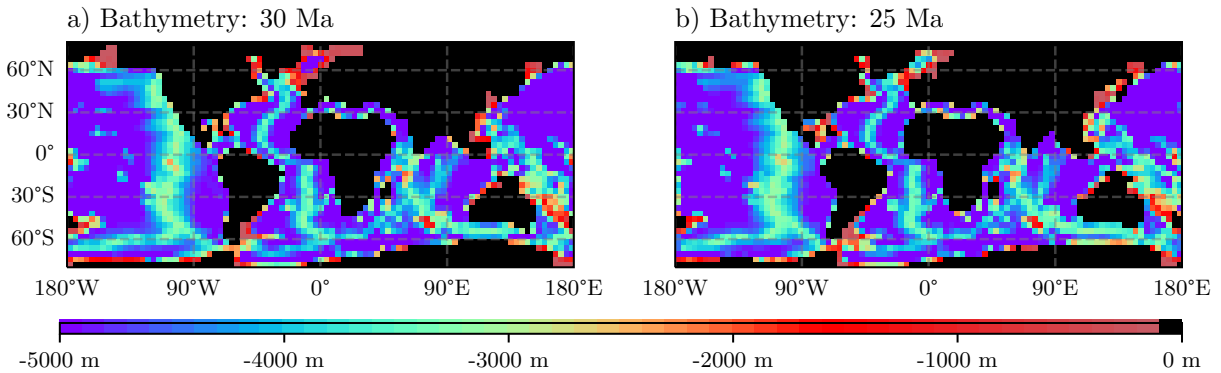


Figure 11: Oligocene bathymetries, black squares show the land mask used. The bathymetries for **(a)** 30 Ma here the Drake passage is opened, this detaches south America from Antarctica and allows the onset of the ACC **(b)** 25 Ma where the Thetys Seaway is seen to be slowly shrinking.

2.3.4 Miocene

The Miocene is characterized by the slow closure of the Thetys seaway. It had been slowly decreasing in size since the beginning of the Eocene and finally fully detaches the northern passage of flow between the Mediterranean and the Indian ocean from 15Ma onward(Hamon et al. 2013). Another feature that is not captured particularly well by this model but should definitively be mentioned, is the decrease in the size of the Indonesian passage. Which is mainly due to the onset of the volcanic islands we know today.

2.3.5 Pliocene

In the Pliocene the panama passage is finally closed off (Molnar 2008; Pindell et al. 1988). This co-

incides with the present-day situation. Due to the closure the mid latitude throughflow between the Atlantic and Pacific basins is believed to have started. The throughflow in the panama seaway is believed to have reversed in direction with the onset of the decrease in size and subsequent closure of the Thetys seaway (von der Heydt and Dijkstra 2006; Omata and Dijkstra 2003). Something that will be studied more closely in the discussion of our results. Also it is of note that the present day bathymetry used here was made using the same method as the other bathymetries. This decision was made over reusing the existing bathymetry used by the standard 4-degree model. This was done to make a better discussion possible.

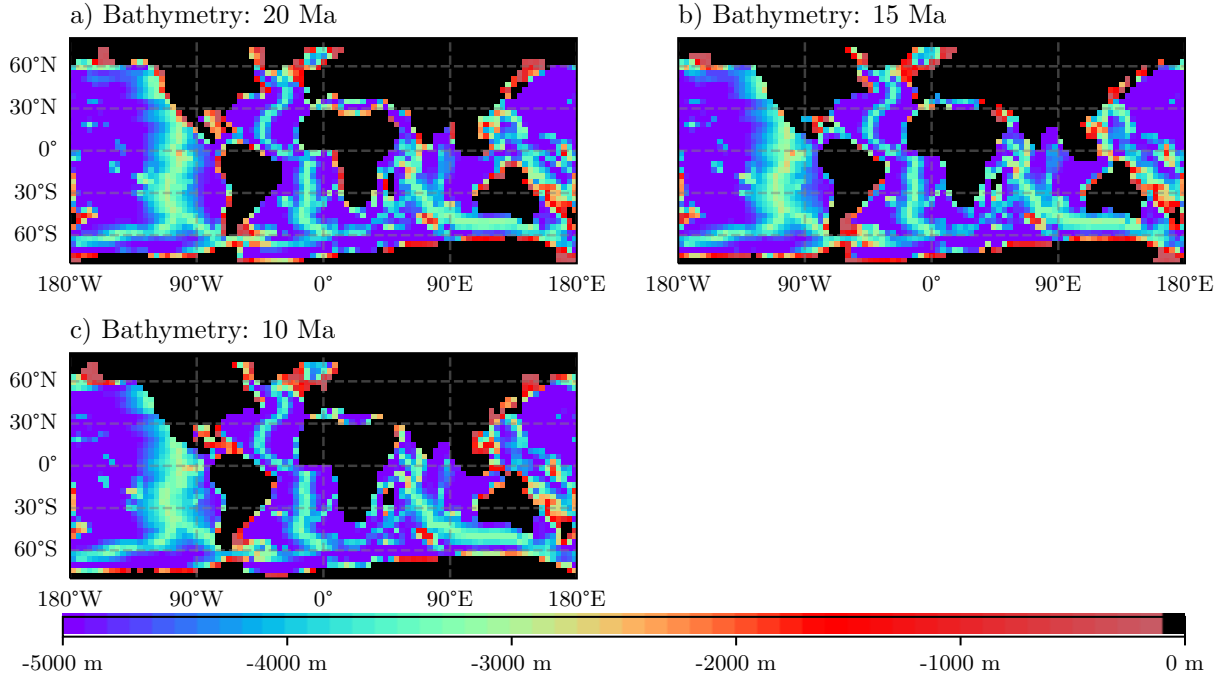


Figure 12: Miocene bathymetries, black squares show the land mask used. The bathymetries for (a) 20 Ma. (b) 15 Ma Here, the closure of the Thethys Seaway is seen which connects the African continent to the Eurasian continent and stops the northern flow of water between the Indian and Atlantic Oceans. (c) 10 Ma Here the panama seaway is seen to become much more shallow. Also the Indonesian passage has shrunk drastically in this period.

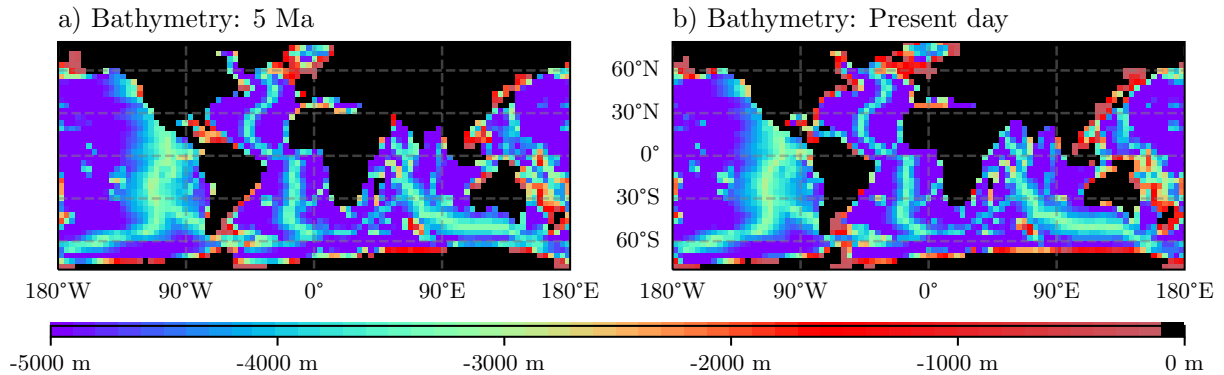


Figure 13: Pliocene bathymetries, black squares show the land mask used. The bathymetries for (a) 5 Ma where the panama passage is closed linking the north and south American continents. (b) The present day situation.

3 Results

3.1 Model runs

The model ran for 500 years for each of the 14 timesteps. Accounting for a total of 7000 years of model time. The timings are shown in table 2. We see that the total integration time is quite long but in general manageable. We note that it would have been possible to significantly speed up our work by using many nodes in parallel instead of a single node in succession. This would be required for higher resolutions but was not attempted here. As a metric for the stability of the model, we look at the globally averaged salinity and temperature change over time. This tells us the drift of the model. In table 2 we see the drift over the last 10 years of integration. We see that all of the models seem to have a drift of less than $10e-4^{\circ}C$ per year and a salinity drift less than $10e-4psu$ per year.

Year	$\Delta time$	time	ΔT	ΔS
present day	1'01"	8:30	-2.1978	-1.8629
5Ma	1'01"	8:30	-2.8292	-2.5038
10Ma	1'01"	8:30	-2.7764	-1.8219
15Ma	1'02"	8:40	-6.1497	-2.6299
20Ma	1'01"	8:30	-5.3202	-1.9109
25Ma	1'02"	8:40	-5.3201	-1.9341
30Ma	1'03"	8:30	-3.0994	-1.5755
35Ma	1'00"	8:30	-0.3163	-1.6289
40Ma	1'02"	8:40	-5.1253	-1.7728
45Ma	1'00"	8:20	-5.1196	-1.7066
50Ma	1'00"	8:20	-4.9925	-1.6592
55Ma	1'01"	8:30	-4.9158	-1.6586
60Ma	1'02"	8:40	-5.5853	-1.6902
65Ma	1'03"	8:50	-6.3302	-1.8980

Table 2: $\Delta time$ is the time per integration in minutes'seconds". $time$ is the time in hours:seconds for each run. ΔT is the average temperature gradient for the last 10 time steps in $10e-4^{\circ}C$ per year. ΔS is the average salinity gradient for the last 10 time steps in $10e-4psu$ per year.

3.2 Control setup

To get an understanding of the quality of the model and thus if any of the results resemble reality, one can compare the present-day setup of the model to an existing model with realistic forcings. Also, the model can be compared to another similar higher resolution model. This can be a useful tool to see what aspects of the present-day situation are cap-

tured by the model and more importantly which nuances are lost. General circulation models with a resolution comparable to the model used in this paper often loose major features having to do with the overturning circulation (Stone and Risbey 1990). Especially the restoring boundary conditions at the surface are troublesome where capturing artifacts of the thermohaline circulation is highly dependent on surface salinity and temperature profiles. This dependence is even further complicated by the highly idealized forcings used here (section 2.2.3). To get a qualitative look at the error introduced in our model, the BSF and the MOC outputs are studied together with their temperature profiles. We compare our control setup with a run of our model with the original ECMWF 2020 forcings scaled to 4-degrees. These are the same forcings used as a basis for making the idealized forcings as mentioned in section 2.2.2.

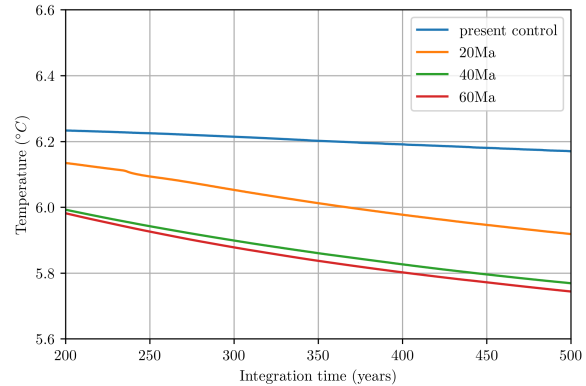


Figure 14: Total globally averaged temperature ($^{\circ}C$) for Present day (blue), 20Ma (orange), 40Ma (green) and 60Ma (red). From 200 to 500 years of integration. A drift is still observed after 500 years of integration but the models do all appear to converge.

3.2.1 BSF control

To look at the quality of the BSF we compare the barotropic stream function with the control(fig. 15). Here we see quite a few differences. Notably, the strength of the gyres is much weaker in our simplified forcings case. This can mostly be explained by the generally weaker wind stresses in these regions. Also, in our simplified model there is a notable absence of the sub polar gyre in the northern Atlantic. The difference in strength of the subtropical gyres is about $10Sv$ on average. Reaching a $20Sv$ difference in the subtropical gyre in the Indian ocean.

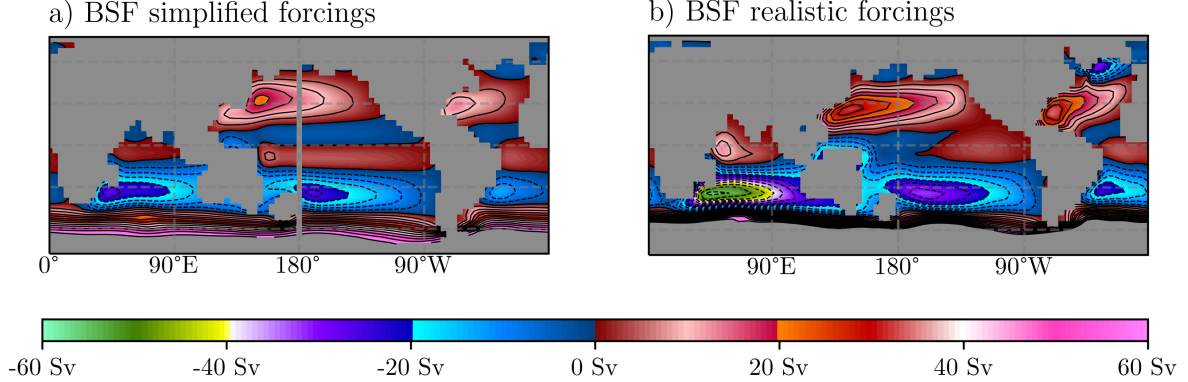


Figure 15: Barotropic stream function with contours every 5 Sv. For **a)** the simplified forcings based on the ECMWF-1° as explained in section 2.2.2 and **b)** realistic ECMWF-4° forcings (ECMWF 2015)

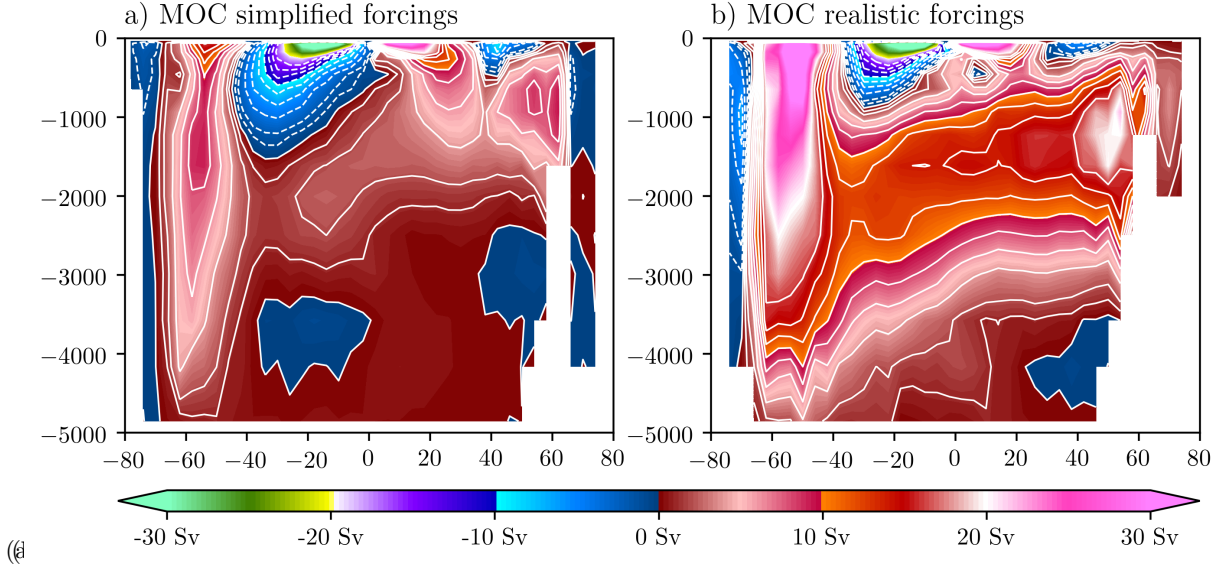


Figure 16: MOC stream function with contours every 2 Sv. For **a)** the simplified forcings based on the ECMWF-1° as explained in section 2.2.2 **b)** realistic ECMWF-4° forcings (ECMWF 2015). Negative values (dashed lines) indicate counterclockwise circulation. Here a large difference between the forcings is clearly visible

3.2.2 Quality of the MOC

Next, we look at the MOC stream functions and compare them between the two models. Here we must note the difference in geometry between the two models. This is because we use an interpolated version in the simplified forcings case. Our geometry is subsequently different from the geometry used from the ECWMF-4° forcings. In fig. 16 we see the MOC stream function for the simplified

and realistic models. Here the real problem of using simplified forcings is visible. The overturning circulation with the simplified forcings is extremely weak compared to the overturning circulation with simplified forcings. Compared to the model with realistic forcings in fig. 16b we see that the NADW cell is much weaker in fig. 16a.

We note that several key features are not captured by both models. The first, most striking feature is the complete absence of the AABW cell.

This is a common feature of low-resolution models used here. Furthermore it is noted that the absence of accurately simulated sea ice in both models contributes further to the quality of the southern ocean simulations. We also see a very large cell in the southern ocean around $60^{\circ}S$. This is a purely wind-driven cell not seen in the more realistic overturning from fig. 5. It is known as the "Deacon cell" (Sverdrup, Johnson, and Fleming 1942; Deacon 1933).

3.3 Passage throughflow

As discussed in section 2.2.7 the passage throughflow is calculated by using the BSF. To do this a suitable location was chosen for each time step and passage such that there are no boundaries next to the passageways. This method is the same for each of the passages, noting that only zonal flow was studied. Thus we can study the effect of changes in bathymetry on the relative strength of the flow. The studied passageways are labeled in fig. 8. The computed throughflow can be seen in fig. 17. The onset of the ACC is visible. With the onset of the ACC a reversal of flow between the Indian and Pacific oceans is seen. Showing that due to the northward movement of Australia and the deepening of the drake passage the total volume transported by the ACC grows dramatically over time. Furthermore, it can be seen that the opening of the drake passage causes the flow through the Aghulas passage to reverse in direction. Also, the throughflow through the Panama passage is shown to slow due to both the onset of the ACC and the closure of the Tethys Seaway. Finally the direction of flow through the Panama passage is reversed after 15Ma due to the total closure of the Tethys Seaway. The reversal of the Indonesian throughflow observed by Mulder et al. 2017 is not observed with total throughflow always moving water east to west. This is however in agreement with the flow found by Omta and Dijkstra 2003 in a shallow-water model. Note, however, that the bathymetries used by their paper deviate dramatically from the ones used here.

To get a better understanding of the flows, we look at a vector field showing the direction of horizontal water displacement for each of the timesteps. This is done by making a weighted mean of the hor-

izontal flow field for each layer weighted by the volume of each grid cell. Each vector represents the total flow for each full depth grid cell. Thus showing the total velocity field of the ocean and the subsequent direction of water displacement. The velocity fields are plotted in fig. 18. Here the ACC is again very noticeable. The reversal of flow through the Panama passage at 15Ma is the most interesting result here. Where here we find the closure of the Thetys seaway to be the main factor. However, the reversal only occurs after the closure of the seaway. This result is similar to what was found by Omta and Dijkstra 2003 where the flow reversal was also observed to coincide with the closure of the Thetys Seaway.

The largest changes in the velocity field are observed in the Indian Ocean. The Indian continent moves northward at a very fast pace. After 55 Ma the flow through the passage north of the Indian continent is massively reduced and instead, the water flows east of the continent into the Tethys Seaway. No current circulating India is observed in any of the time steps. The position of the Indian continent does however seem to have a strong influence on the strength of the Aghulas sub-tropical gyre. This can probably be explained by the amount of water that is transported through the Tethys seaway. A closer inspection of this gyre can be found in section 3.4.

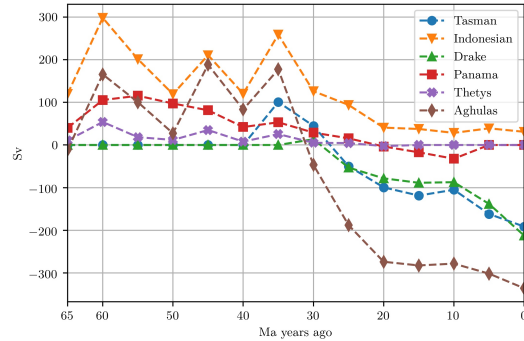
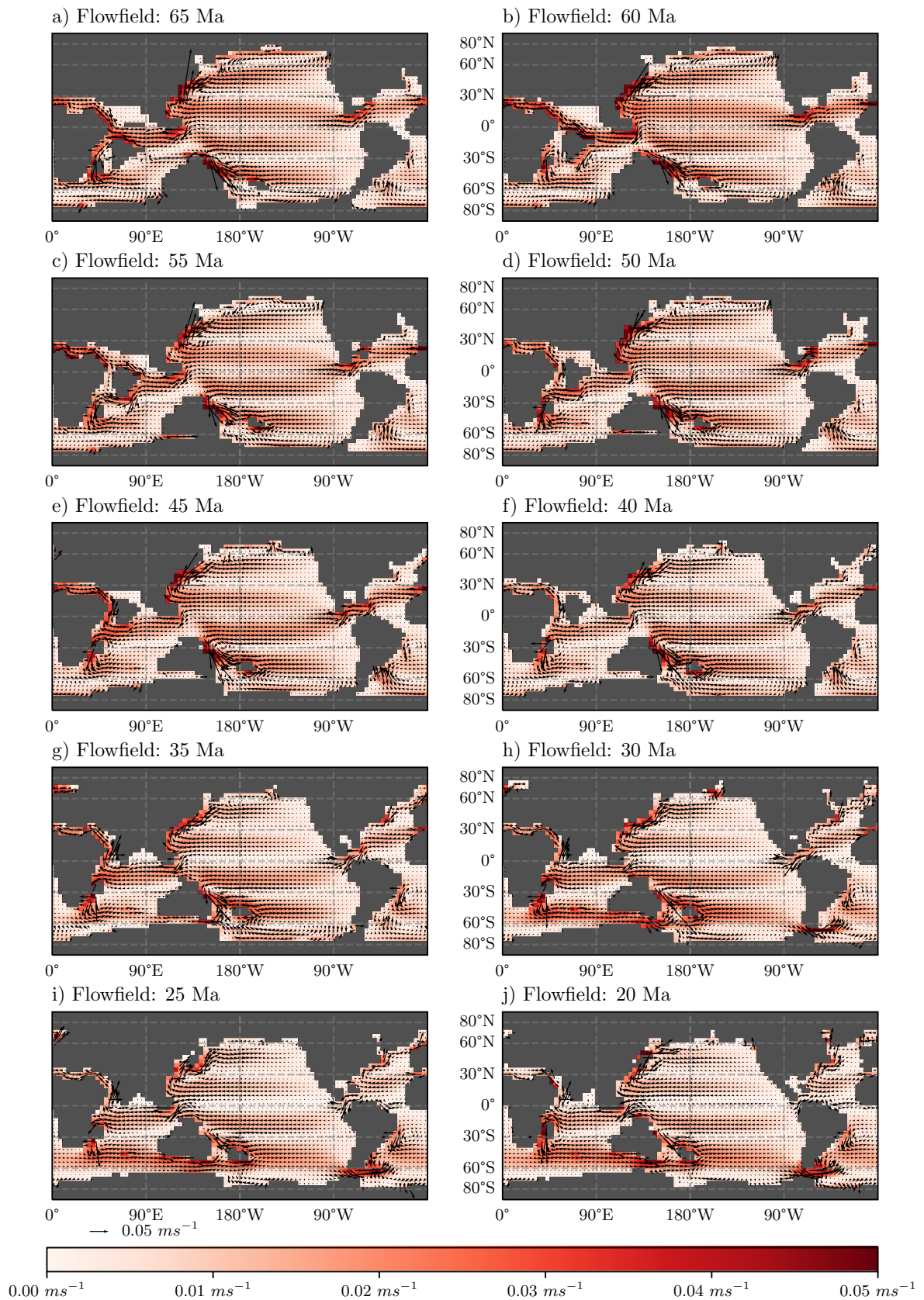


Figure 17: Total volume transport in Sverdups ($10^6 m^3 s^{-1}$) running from 65 milion years ago to the present day situation. Positive values indicate transport to the west. Passage names as defined in fig. 7.



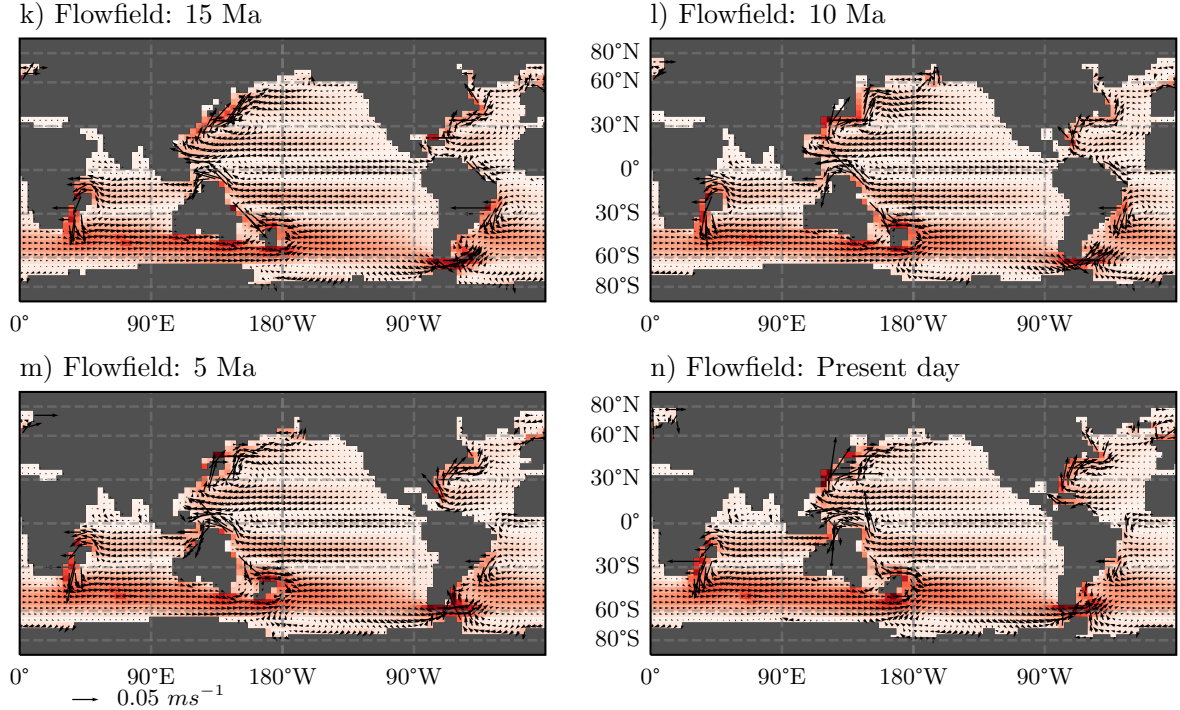


Figure 18: Flow field for each time step as a weighted mean showing the average velocity of each vertical water column in ms^{-1} . Serves to indicate flow direction and relative strength in the oceanic basins. Also serves as a basis to compare results with the shallow water model in Omta and Dijkstra 2003

3.4 Barotropic Stream function

Next, we will look at the barotropic stream function for each of the time steps discussed in this paper. Some of the flows that are discussed in this section are closely related to the flows explained in section 3.3. Here we will have a stronger focus on the gyres seen in the ocean and their relative strength in a time sense. Each of the oceanic basins is discussed in detail. An overview of each of the barotropic stream functions can be seen in fig. 20. The boundary values of the BSF are not shown here. This is due to the previously stated fact that they are excluded from the model output produced by Veros. It must however be noted that this does not mean that flows through the passages are not modeled. In this case, the barotropic stream function serves only to see the major ocean gyres and how water is transported in these gyres.

3.4.1 Indian Ocean

The Indian ocean and especially the Indian Continent moving northward seems to be one of the most interesting artifacts of these simulations. When the Indian continent is still within the subtropical gyre

range in the early Paleocene. We see that it has a large blocking effect on the subtropical gyre in the Indian ocean. We also see, as observed in the Flow patterns for each of the basins, a change from current moving north over India to moving east and then up towards the Atlantic basin. Something that is similarly observed in Omta and Dijkstra 2003. However as noted in section 2.2.7 we do not observe a the often shown circum-India current (Omta and Dijkstra 2003; von der Heydt and Dijkstra 2006). In the Paleocene, the Indian continent seems to be the most influential in establishing the ocean gyres. The stark contrast between 65 and 60Ma BSF can be explained due to the Kohistan-Ladakh Arc island ridge north of India. These islands block the flow from developing a strong current around the Indian continent.

3.4.2 Pacific Ocean

The Pacific Ocean is of particular interest in this case. One of the main things that we see is a large variability in the strength of the southern subtropical gyre. There appears to be a variability in the order of $\pm 20Sv$. The variability is most pro-

nounced when the ACC is not yet fully developed and is most pronounced in the Paleocene and early Eocene. The transport is particularly extreme at times where the Thetys throughflow is the larger. The size of the southern subtropical gyre seems to relate to the Thetys values seen in Figure 17 on page 13. Here we see a current around the planet through the Thetys, Indonesian, and Panama passages. This can explain why such a large positive stream function can be seen in the southern Pacific.

3.4.3 Atlantic Ocean

The Atlantic Ocean seems to be the least influential in most of the timesteps studied here. This is

in large part thanks to the fact that the Atlantic basin is relatively small in the Paleocene growing slowly over time. The one gyre of note in the Atlantic which exists until the onset of the ACC is the southern subpolar gyre. This gyre shows similar variability to the Gyres in the Pacific and Indian oceans. The onset of the ACC also seems to coincide with the growth of the southern subtropical gyre. Also, the northern subpolar gyre is hardly visible here at all. This is likely due to low resolution used by this model not being able to have proper in and outflow of the northern arctic sea.

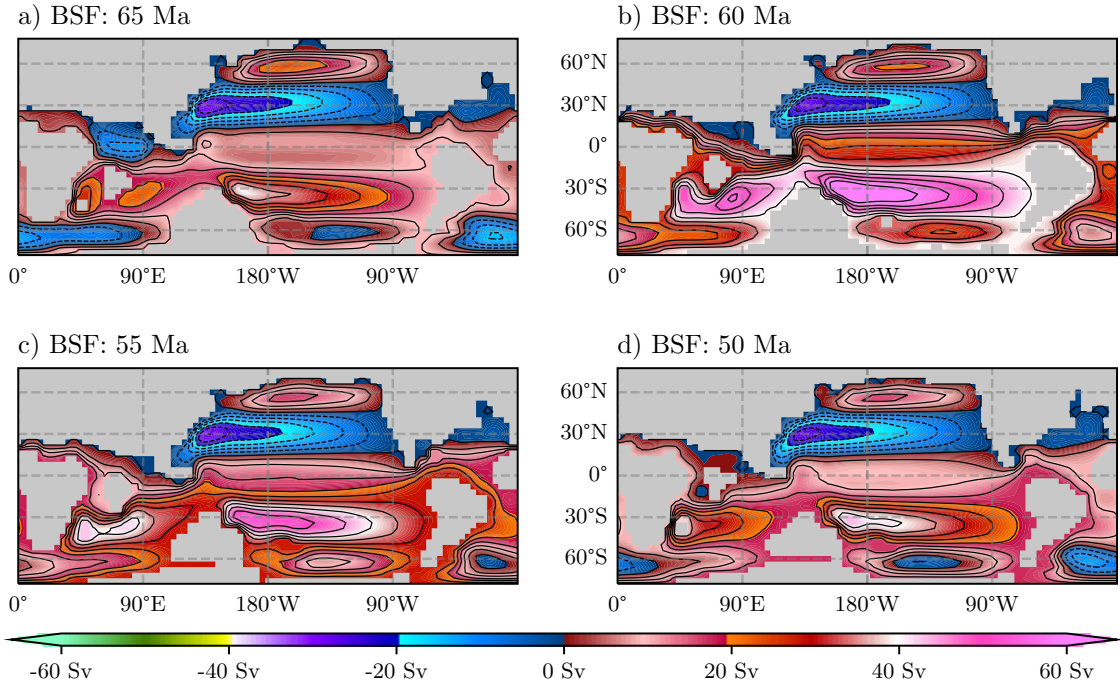


Figure 19: Barotropic Stream Function with contour lines every $5Sv$ for the period from 65 Ma to 40 Ma. Note that the boundary values of the BSF are shown here but that the drake passage is closed and that there is no flow is propagating through the passage.

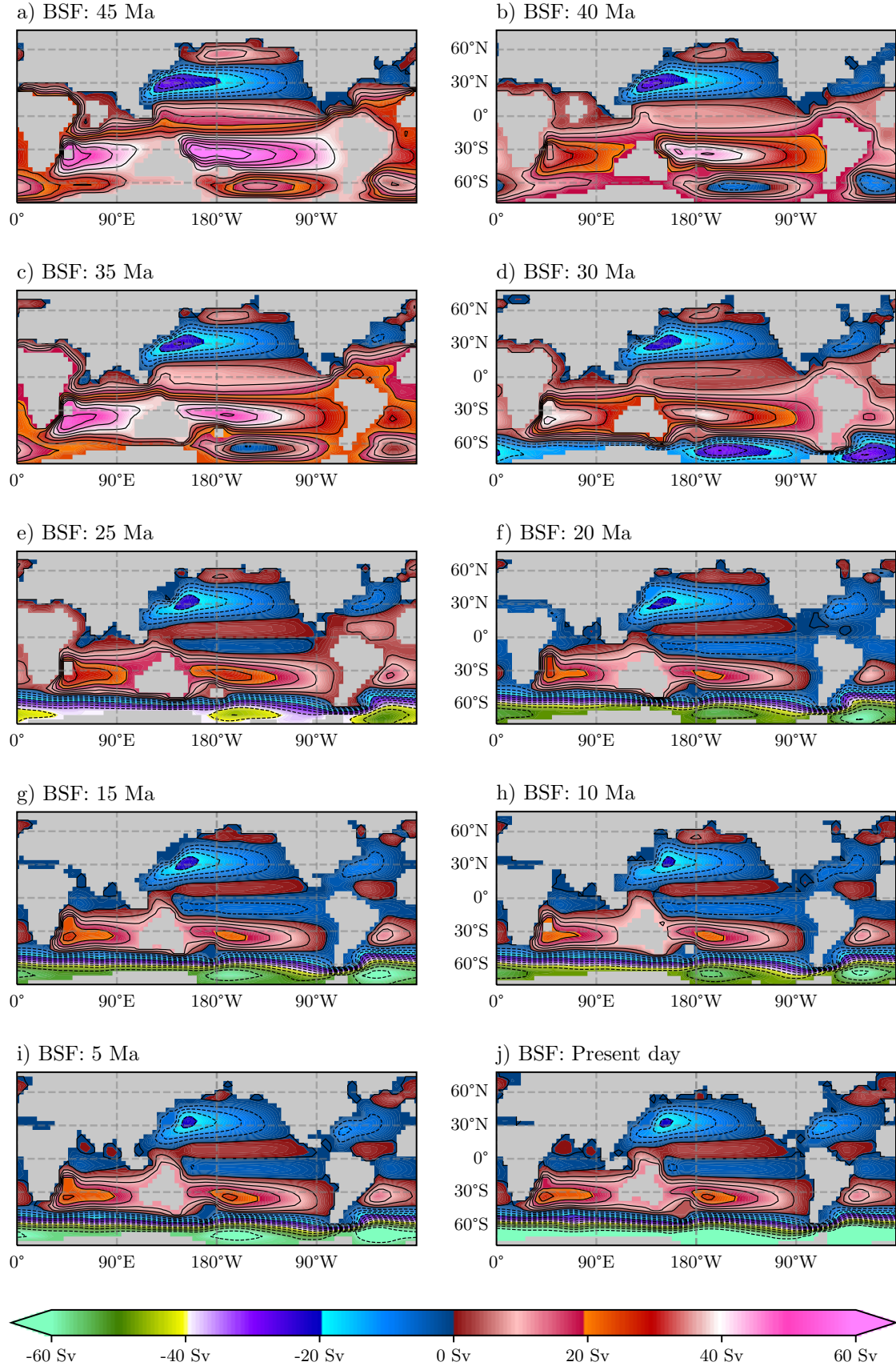


Figure 20: Barotropic Stream Function with contour lines every $5Sv$ for the period from 35 Ma to the present day configuration. Note that the boundary values of the BSF are shown here but that the panama passage is closed after 5 Ma and no flow is propagating through the passage.

3.5 MOC Stream function

Next we will do an analysis on the Global Meridional overturning current stream function (MOC). As mentioned in section 2.2.5 these values will probably not result in a very realistic picture of the overturning circulation. However it still gives us a rough general idea of the deep ocean flows of the thermohaline circulation. The main focus in this section will be on wind driven circulations as they seem to be quite accurately captured as discussed in section 3.2.2.

The MOC stream function we observe little variability until the onset of the "ACC-like" cell at 35Ma (fig. 21). However we do observe some changes in the period extending to the late Eocene. In the Paleocene one of the most interesting features seen in the MOC stream function is a southern cell extending from the equator to the Antarctic continent and a mirrored cell in the north. Almost mirroring around the equator. However the southern cell is observed to be stronger with a weaker A strong ($9Sv$) southern cell exists until 55 Ma where its extend is not as far south.

3.5.1 Eocene

In the Eocene we observe little difference to the stream function in the Paleocene. The most interesting feature is the southern subpolar gyre. Which starts to extend downwards like the ACC in the present day. The antarctic bottomwater cell is subsequently significantly reduced in strength. The origin of this "ACC-like" cell at 35Ma is attributed to the opening of the Tasman passage in the bathymetry. This is similar to the open Tas-

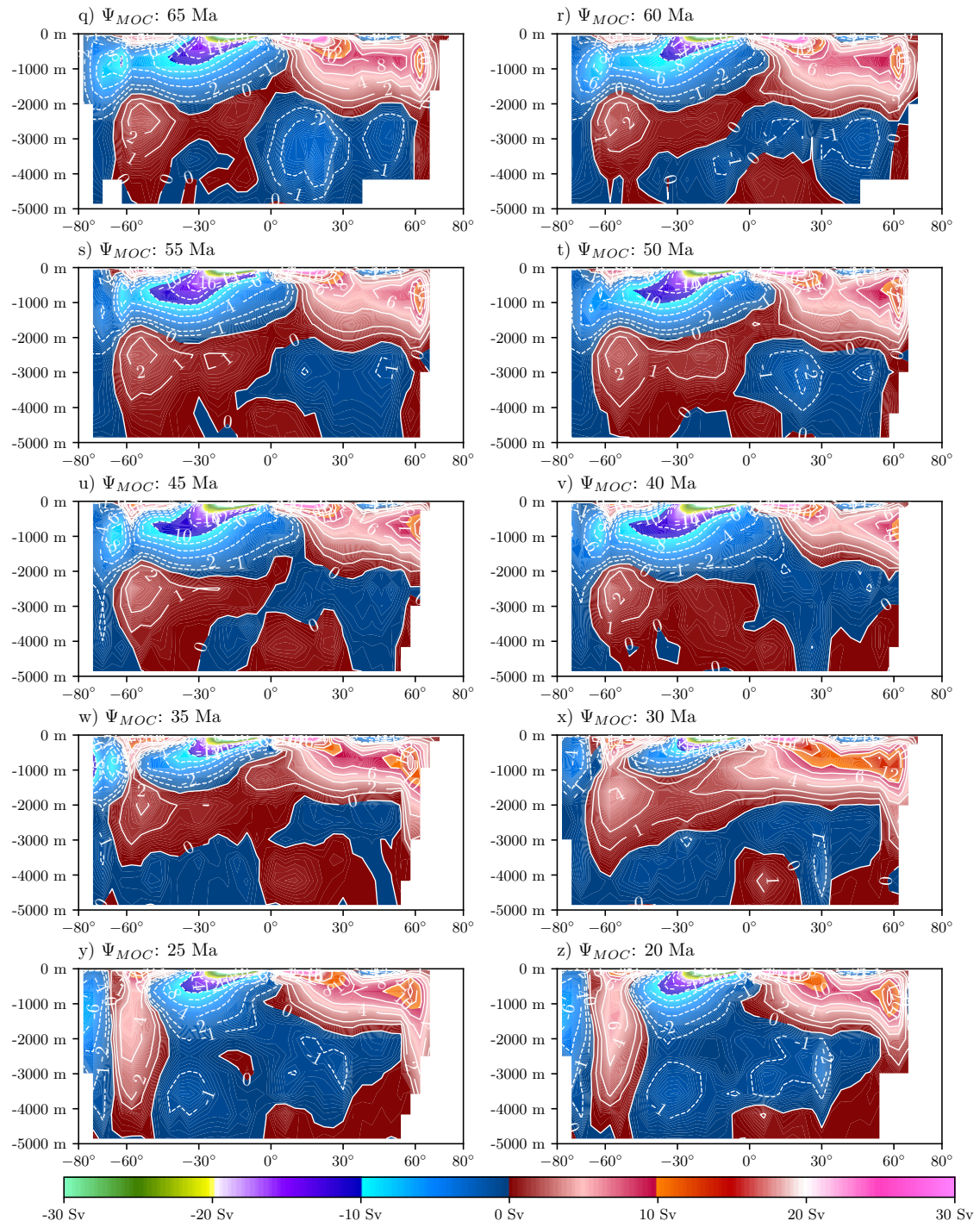
man and closed Drake passage case shown by Sijp, England, and Huber 2011.

3.5.2 Oligocene

The Oligocene is characterized by the strong onset of the ACC and a subsequent decrease in size of the south polar cell. It being "pushed" aside due to the strong ACC currents. Another interesting artifact of this is that in the 30Ma setup a kind of overturning current is observed. This is however not shown in the 25 and 20 Ma time steps. It should be noted that the deep water cells ($j-2000$ m) in all of these are still too weak to be of any realistic value. The Oligocene does seem to harbour some of the strongest Polar cells in any of the models. This was not necessarily observed in the Pictures of the BSF.

3.5.3 Miocene

The Miocene shows some of the main features of the MOC. One of these is the overturning current previously mentioned. It is however important to note that it is still really weak compared to other models with more depth layers and observations (von der Heydt and Dijkstra 2006). Probably due to the fact that the overturning circulation in the Atlantic is absent in this model. This may simply be a case of boundary conditions but could also be explained by the relatively weak SSS forcings in the Atlantic compared to real world values. In the last 15 Ma we see very little change overall in the MOC stream function. We see mostly fluctuations in the northern sub polar cell.



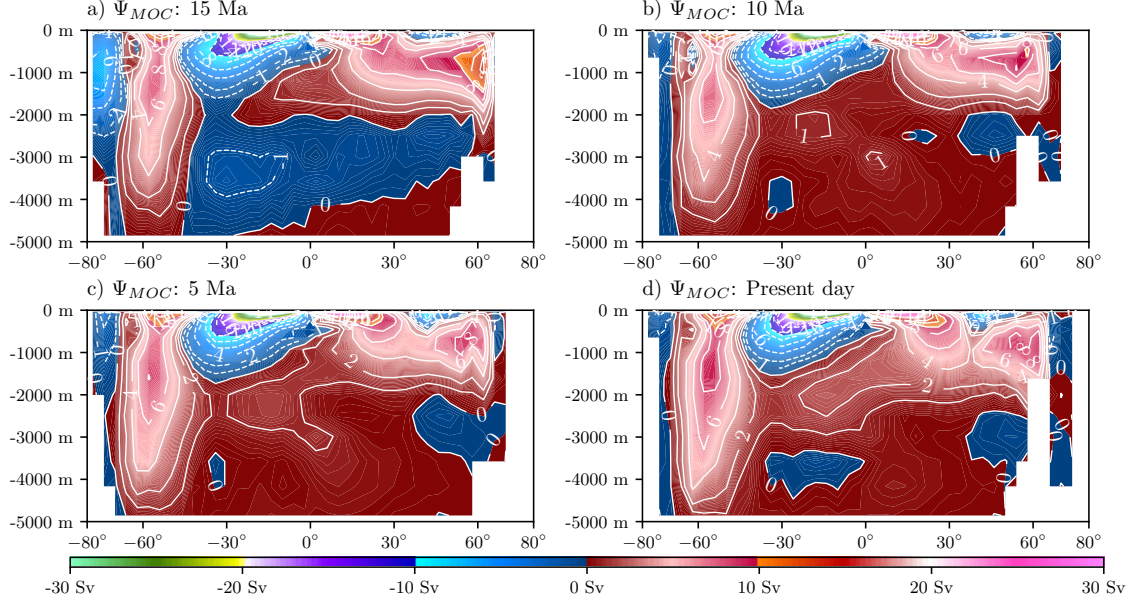


Figure 21: Meridional overturning circulation stream function with contours every 2 Sv and an extra contour for -1Sv and 1Sv . Dotted contours indicate negative values. The Deacon cell appearing with the onset of the ACC is particularly visible here.

3.6 Temperature and Salinity

To get a better picture of the changes that occur during the time periods the differences in sea temperature and salinity between the models and the original begin conditions are compared. The sea surface temperature and salinity are not used here because of the restoring boundary conditions. Instead the results at a depth of -245m are used. It is important to note that these restoring boundary conditions with the simplified forcings make any discussion on the thermohaline circulation to be of limited value.

3.6.1 Salinity Changes

First, looking at the salinity profiles in fig. 22 the gyres seen in the BSF are clearly visible(section 3.4). Little other changes can be deduced. Especially in the pacific where only marginal changes are observed. However, the closure of the Thetys Seaway can be seen in both the Atlantic and Indian basin. Fresher water from the arctic is transported south when the Thetys transport is low and the northern subtropical gyre is started. Also a variability in the Indian ocean is seen which coincides with the variability in the Thetys Seaway throughflow. Indicating that a connection between these exists, allowing salt water to

flow away from the Indian basin. Also the Eocene-Oligocene boundary between 35 and 30Ma shows a change in salinity in the southern subpolar region. A connection between the subpolar gyres seen in the BSF due to the opening of the Tasman and Drake passage is clear here. Making the Antarctic region slightly more saline.

3.6.2 Temperature Changes

To look at the temperature changes we look at the profiles compared to the initial conditions (fig. 23). Again the major ocean gyres are visible. Here the strong influence of the restoring boundary conditions is visible. Similar to what was observed in the Salinity profiles there is a variability observed in the Eocene-Oligocene boundary. The ACC-like cell described in section 3.5.1 seems to keep the warm water south. After 35Ma, when the ACC is fully developed the temperature stabilizes again.

In the Indian ocean the influence of the Indian continent's movements is seen. The Indian ocean being a few degrees cooler before the Eocene-Oligocene boundary when India is still detached from Eurasia. Two processes might explain this. First of all, the decrease in throughflow through the Indonesian passage and second of all the reduction of the blocking effect of the Indian continent of the subtropical gyre.

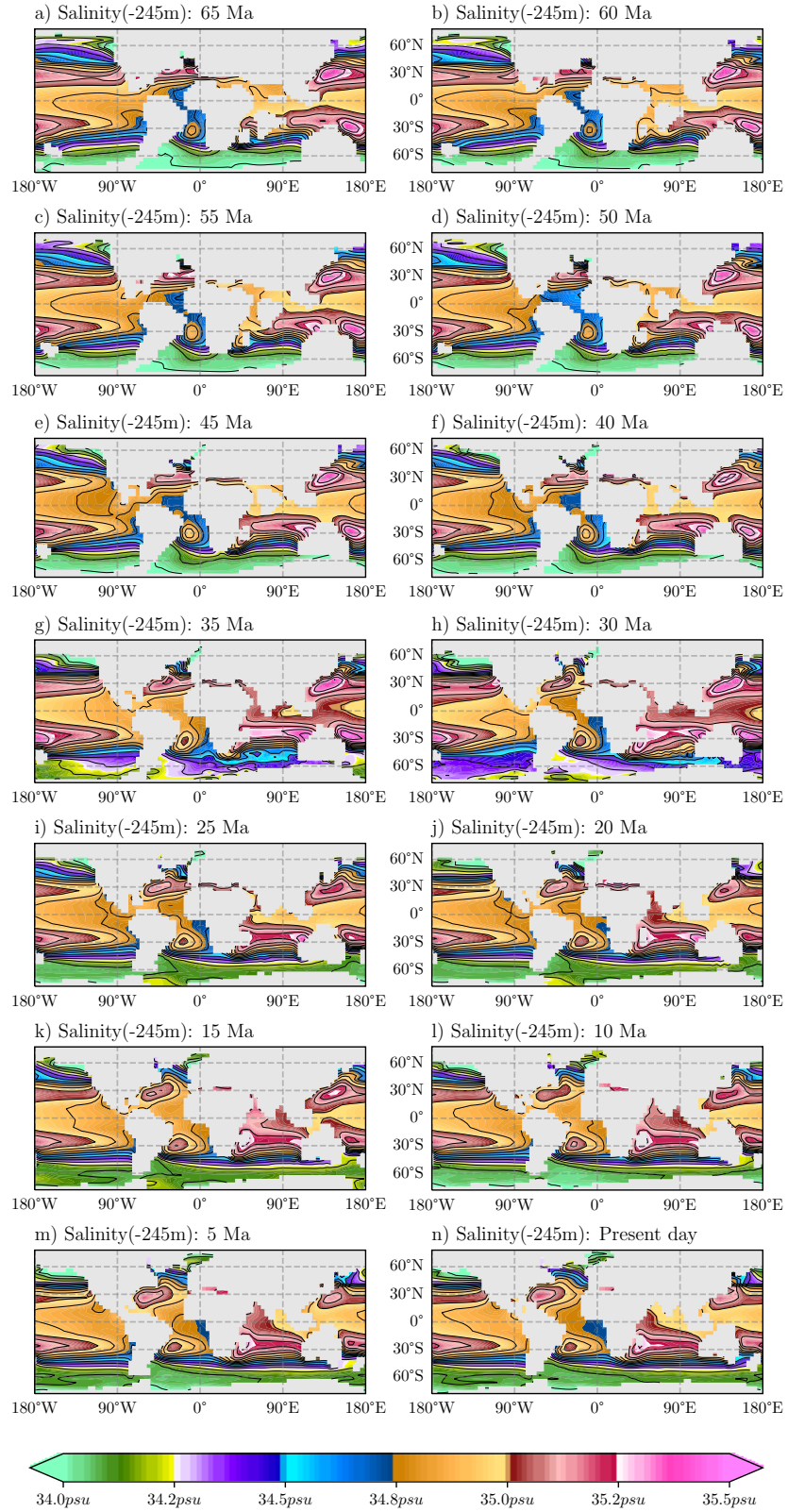


Figure 22: Salinity at 245m depth for each time step.

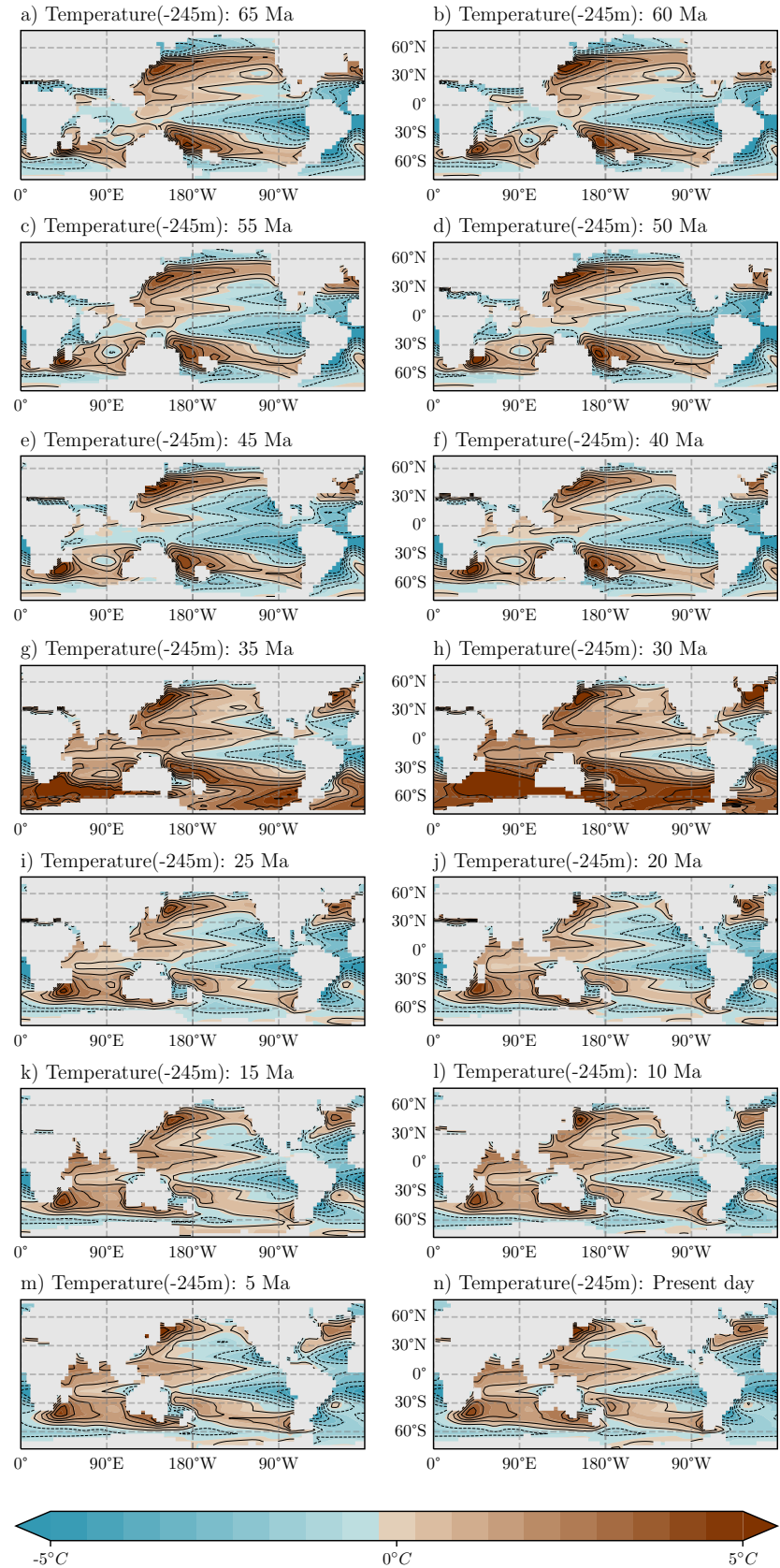


Figure 23: Temperature at 245m depth for each time step.

4 Summary

In this paper, we have presented a simplified approach to the modeling of past climate systems using Veros. This paper focused heavily on simplified forcings of the global oceanic basins. This allows us to efficiently look at the effect of changes in geometry on the major oceanic flows. The results shown here are of relatively low resolution and highly idealized boundary conditions. But they still manage to capture some of the features of more complex models. The integrations were done on a consumer computer showing that it is possible to do even larger ocean simulation research on readily available hardware.

In the barotropic stream functions, we observed high variability between the different integrations. Especially in the Paleocene where it was mainly attributed to the large variation in the Indian ocean. It thus appears that the exact location of the Indian continent may have had profound implications on the past oceanic circulations. In our study of the passage throughflow, we find that there is a flow reversal in the Panama passage after the closure of the Tethys Seaway. Here we also find large variability in the passage throughflows before the onset of the Antarctic circumpolar current. Furthermore, we observe flow reversal in the Aghulas passage occurring simultaneously to the opening of the drake passage.

We were unable to accurately predict the meridional overturning circulation. We do however find some evidence for a total absence of transport over the equator before the onset of the ACC.

In general, we observe a wind-driven circulation that quite accurately manages to capture the changes in volume transport through the major passages. We find that using zonally averaged forcings do have major implications on the strength of the flows but the large scale changes are captured. We can conclude that the simulations were quite successful in capturing the wind-driven circulation but require much higher resolution to be useful in present-day research.

5 Discussion

The method presented here for an alternative to the continuation approach suggested by Mulder et al. 2017 still has quite a few problems. First of all the 4° resolution together with the limited number of depth layers is one of the main problems. The lim-

ited depth layers fail to accurately capture even the present day overturning circulation. Here we note that the same can be said for a model with present day forcings as noted in section 3.2.2. Next, we also note that an ACC strength of just $80Sv$ is a lot lower than the observed $100\text{-}150 Sv$. This can mainly be attributed to the weaker wind forcings in the southern hemisphere. The present day zonal wind forcing being more than 50% stronger.

The possibility of using a 1 or 2 degree Veros model for this paper was extensively explored. But issues often arose with the exact values of constants and frequent invalid value errors to do with eddy kinetic energy could not be fixed in time for this paper.

The 4 degree model also took quite a bit of time to be adapted for the customized forcings and bathymetries. This is due to the fact that the method for determining boundary conditions for islands would often find more islands than exist in the model. Resulting in having to customize each setup individually for its bathymetry to accept the islands present. This is also why $180^{\circ}E$ was used as the boundary longitude instead of the default 0° .

Another major thing that is generally neglected in this paper is the total absence of change in surface forcings. Even though it is known that these change drastically even in short time spans. We also have some general knowledge of global average temperature for the time period discussed here. However the search for a dataset for each time step has proven futile. Often large uncertainties exist. This left us with the decision to not bother with any changes in the forcings. Even though there have been massive changes in the time period discussed here. Coupled with the sensitive nature of GCM's we suggest taking the results in this paper with a grain of salt.

A lot of future research is possible in the topic of oceanic throughflow. More accurate bathymetries are being produced due to breakthroughs in geological techniques (Baatsen et al. 2016). These, coupled with a higher resolution model will probably result in even more accurate depictions of the past oceanic systems. Research on this topic is of particular importance because of the present day observed changes in strength of the MOC.

6 Acknowledgments

This paper would not have been possible without the extensive support of Dr. Anna von der Heydt,

who provided valuable input on every single one of the many hurdles that had to be succumbed. I would also like to thank Dr. Michiel Baatsen for providing the bathymetry datasets used in this paper, Prof. Dr. Markus Jochum for providing valuable insight into Veros and Laurits Andreasen for helping with many of our questions and attending our virtual meetings.

References

- [1] Jean Besse and Vincent Courtillot. “Apparent and true polar wander and the geometry of the geomagnetic field over the last 200 Myr”. In: *Journal of Geophysical Research: Solid Earth* 107.B11 (2002), EPM–6.
- [2] Howie D. Scher and Ellen E. Martin. “Timing and Climatic Consequences of the Opening of Drake Passage”. In: *Science* 312.5772 (2006), pp. 428–430. ISSN: 0036-8075. DOI: 10.1126/science.1120044.
- [3] D. N. Schmidt. “The closure history of the Panama Isthmus: Evidence from isotopes and fossils to models and molecules”. In: *ResearchGate* (2007), p. 429444. URL: https://www.researchgate.net/publication/282323290_The_closure_history_of_the_Panama_Isthmus_Evidence_from_isotopes_and_fossils_to_models_and_molecules.
- [4] Wallace S Broecker. “The great ocean conveyor”. In: *Oceanography* 4.2 (1991), pp. 79–89.
- [5] Meir Abelson and Jonathan Erez. “The onset of modern-like Atlantic meridional overturning circulation at the Eocene-Oligocene transition: Evidence, causes, and possible implications for global cooling”. In: *Geochemistry Geophysics Geosystems* 18 (May 2017). doi: 10.1002/2017GC006826.
- [6] T. E. Mulder et al. “Efficient computation of past global ocean circulation patterns using continuation in paleobathymetry”. In: *Ocean Model. 115* (2017), pp. 77–85. ISSN: 1463-5003. DOI: 10.1016/j.ocemod.2017.05.010.
- [7] Dion Hafner et al. “Veros v0.1 - a fast and versatile ocean simulator in pure Python”. In: *Geosci. Model Dev. 11.8* (2018), p. 3299. ISSN: 1991-959X. URL: <https://go.gale.com/ps/anonymous?id=GALE%7CA550451036&sid=googleScholar&v=2.1&it=r&linkaccess=abs&issn=1991959X&p=AONE&sw=w>.
- [8] *pyOM2 documentation*. [Online; accessed 11. Jun. 2020]. URL: https://wiki.cen.uni-hamburg.de/ifm/T0/pyOM2?action=AttachFile&do=view&target=pyOM2_2.pdf.
- [9] Ralph F. Milliff et al. “Ocean general circulation model sensitivity to forcing from scatterometer winds”. In: *J. Geophys. Res. Oceans* 104.C5 (1999), pp. 11337–11358. ISSN: 0148-0227. DOI: 10.1029/1998JC900045.
- [10] Frank Bryan. “Parameter sensitivity of primitive equation ocean general circulation models”. In: *Journal of Physical Oceanography* 17.7 (1987), pp. 970–985.
- [11] Andreas Schmittner and Thomas F Stocker. “A seasonally forced ocean–atmosphere model for paleoclimate studies”. In: *Journal of climate* 14.6 (2001), pp. 1055–1068.
- [12] ECMWF. *ECMWF | CAMS Climate Forcing Estimates*. 2020.
- [13] James Hansen et al. “Climate sensitivity, sea level and atmospheric carbon dioxide”. In: *Philosophical transactions. Series A, Mathematical, physical, and engineering sciences* 371.2001 (2013). doi: 10.1098/rsta.2012.0294.
- [14] G. Forget et al. “ECCO version 4: an integrated framework for non-linear inverse modeling and global ocean state estimation”. In: *Geosci. Model Dev. 8.10* (2015), pp. 3071–3104. ISSN: 1991-959X. DOI: 10.5194/gmd-8-3071-2015.
- [15] Harald Ulrich Sverdrup. “Wind-driven currents in a baroclinic ocean; with application to the equatorial currents of the eastern Pacific”. In: *Proceedings of the National Academy of Sciences of the United States of America* 33.11 (1947), p. 318.
- [16] R. Alan Plumb John Marshall. “Atmosphere, Ocean and Climate Dynamics: An Introductory Text”. In: San Diego, California: Elsevier Academic Press, 2012. Chap. The wind-driven circulation, p. 214. ISBN: 978-0125586917.

- [17] Michiel Baatsen et al. “Reconstructing geographical boundary conditions for palaeoclimate modelling during the Cenozoic”. In: *Clim. Past* 12.8 (2016), pp. 1635–1644. ISSN: 1814-9324. DOI: 10.5194/cp-12-1635-2016.
- [18] Roy Livermore et al. “Paleogene opening of Drake Passage”. In: *Earth Planet. Sci. Lett.* 236.1 (2005), pp. 459–470. ISSN: 0012-821X. DOI: 10.1016/j.epsl.2005.03.027.
- [19] O. Jagoutz, P. Bouilhol, and Rajeev Upadhyay. “Geology of the Kohistan-Ladakh arc and its relation to the main Himalayan belt”. In: *AGU Fall Meeting Abstracts* (Dec. 2009).
- [20] Lawrence A. Lawver and Lisa M. Gahagan. “Evolution of Cenozoic seaways in the circum-Antarctic region”. In: *Palaeogeogr. Palaeoclimatol. Palaeoecol.* 198.1 (2003), pp. 11–37. ISSN: 0031-0182. DOI: 10.1016/S0031-0182(03)00392-4.
- [21] Sudipta Sarkar et al. “Late Eocene onset of the Proto-Antarctic Circumpolar Current”. In: *Sci. Rep.* 9.10125 (2019), pp. 1–10. ISSN: 2045-2322. DOI: 10.1038/s41598-019-46253-1.
- [22] Yani Najman et al. “Timing of India-Asia collision: Geological, biostratigraphic, and palaeomagnetic constraints”. In: *J. Geophys. Res. Solid Earth* 115.B12 (2010). ISSN: 0148-0227. DOI: 10.1029/2010JB007673.
- [23] N. Hamon et al. “The role of eastern Tethys seaway closure in the Middle Miocene Climatic Transition (ca. 14 Ma)”. In: *Clim. Past* 9.6 (2013), pp. 2687–2702. ISSN: 1814-9332. DOI: 10.5194/cp-9-2687-2013.
- [24] Peter Molnar. “Closing of the Central American Seaway and the Ice Age: A critical review”. In: *Paleoceanography* 23.2 (2008). ISSN: 0883-8305. DOI: 10.1029/2007PA001574.
- [25] James L. Pindell et al. “A plate-kinematic framework for models of Caribbean evolution”. In: *Tectonophysics* 155.1 (1988), pp. 121–138. ISSN: 0040-1951. DOI: 10.1016/0040-1951(88)90262-4.
- [26] Anna von der Heydt and Henk A Dijkstra. “Effect of ocean gateways on the global ocean circulation in the late Oligocene and early Miocene”. In: *Paleoceanography* 21.1 (2006).
- [27] Anne Willem Omta and Henk A Dijkstra. “A physical mechanism for the Atlantic–Pacific flow reversal in the early Miocene”. In: *Global and planetary Change* 36.4 (2003), pp. 265–276.
- [28] Peter H Stone and James S Risbey. “On the limitations of general circulation climate models”. In: *Geophysical Research Letters* 17.12 (1990), pp. 2173–2176.
- [29] ECMWF. *1x1 degree monthly ocean forcings*. https://sid.erae.dk/share_redirect/gsdZADr8to/global_1deg/forcing_1deg_global.nc. Accessed: 2020-02-05. 2015.
- [30] Harald Ulrik Sverdrup, Martin Wiggo Johnson, Richard H Fleming, et al. *The Oceans: Their physics, chemistry, and general biology*. Vol. 7. Prentice-Hall New York, 1942.
- [31] G. Deacon. *A General Account of the Hydrology of the South Atlantic Ocean*. Discovery reports Vol.7, p.171-238. University Press, 1933. URL: <https://books.google.nl/books?id=iObCGwAACAAJ>.
- [32] Willem P. Sijp, Matthew H. England, and Matthew Huber. “Effect of the deepening of the Tasman Gateway on the global ocean”. In: *Paleoceanography* 26.4 (2011). ISSN: 0883-8305. DOI: 10.1029/2011PA002143.

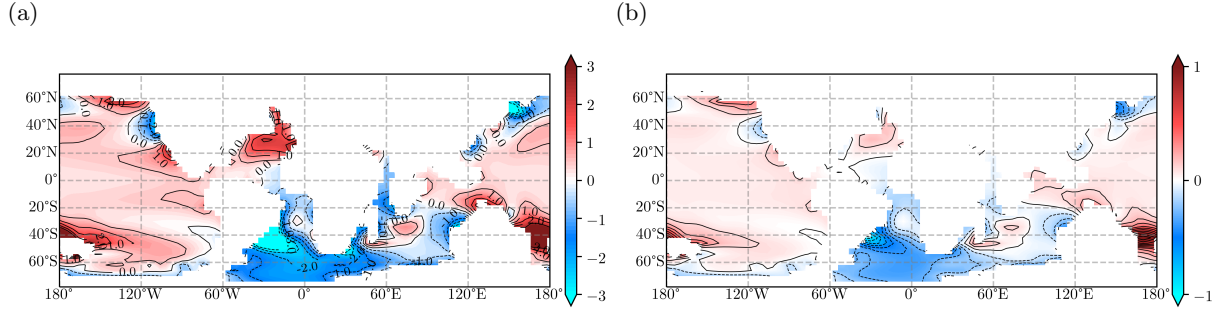


Figure 24: Comparison between late Paleocene (55Ma) and late Eocene (35Ma) for: **a**) Temperature ($^{\circ}\text{C}$) differences (positive values indicate warming) and **b**) Salinity (psu) differences (positive values indicate higher salinity)

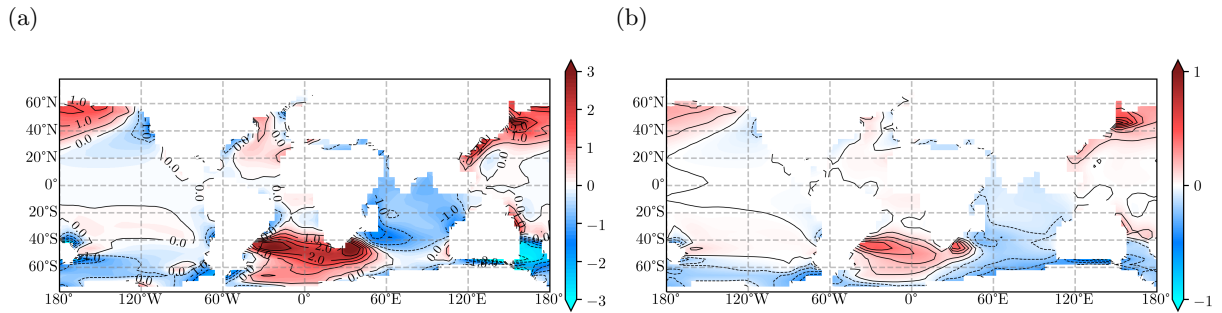


Figure 25: Comparison between late Eocene (35Ma) and early Miocene (20Ma) for: **a**) Temperature ($^{\circ}\text{C}$) differences (positive values indicate warming) and **b**) Salinity (psu) differences (positive values indicate higher salinity)

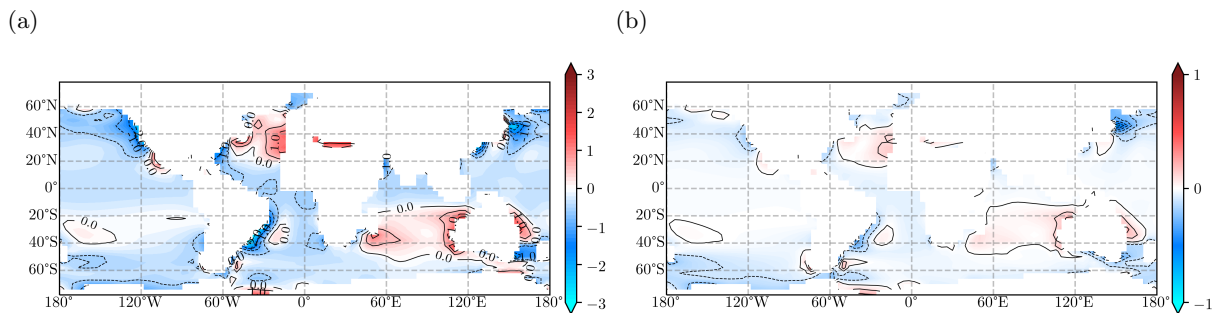


Figure 26: Comparison between early Miocene (20Ma) and late Miocene (10Ma) for: **a**) Temperature ($^{\circ}\text{C}$) differences (positive values indicate warming) and **b**) Salinity (psu) differences (positive values indicate higher salinity)

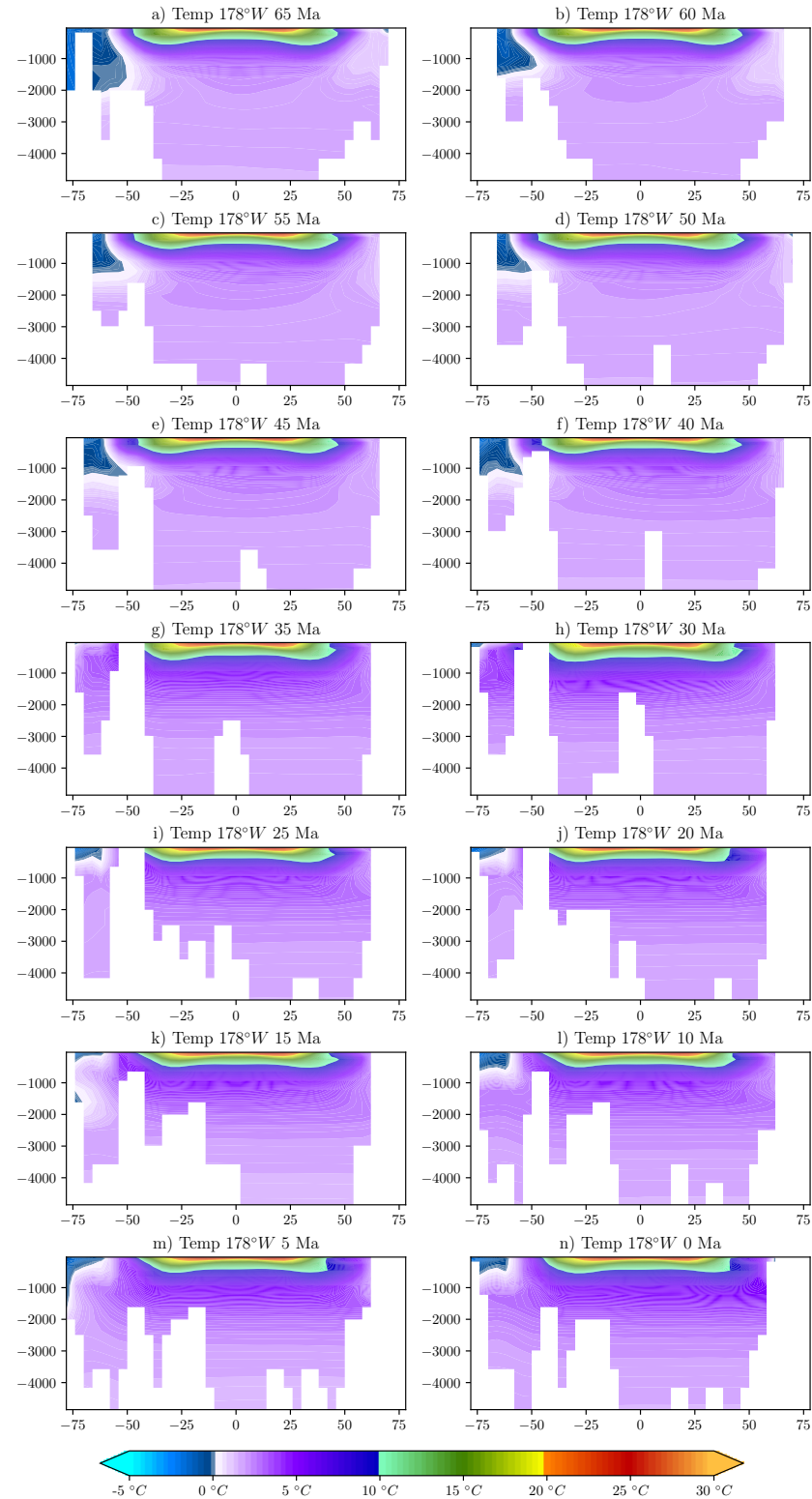
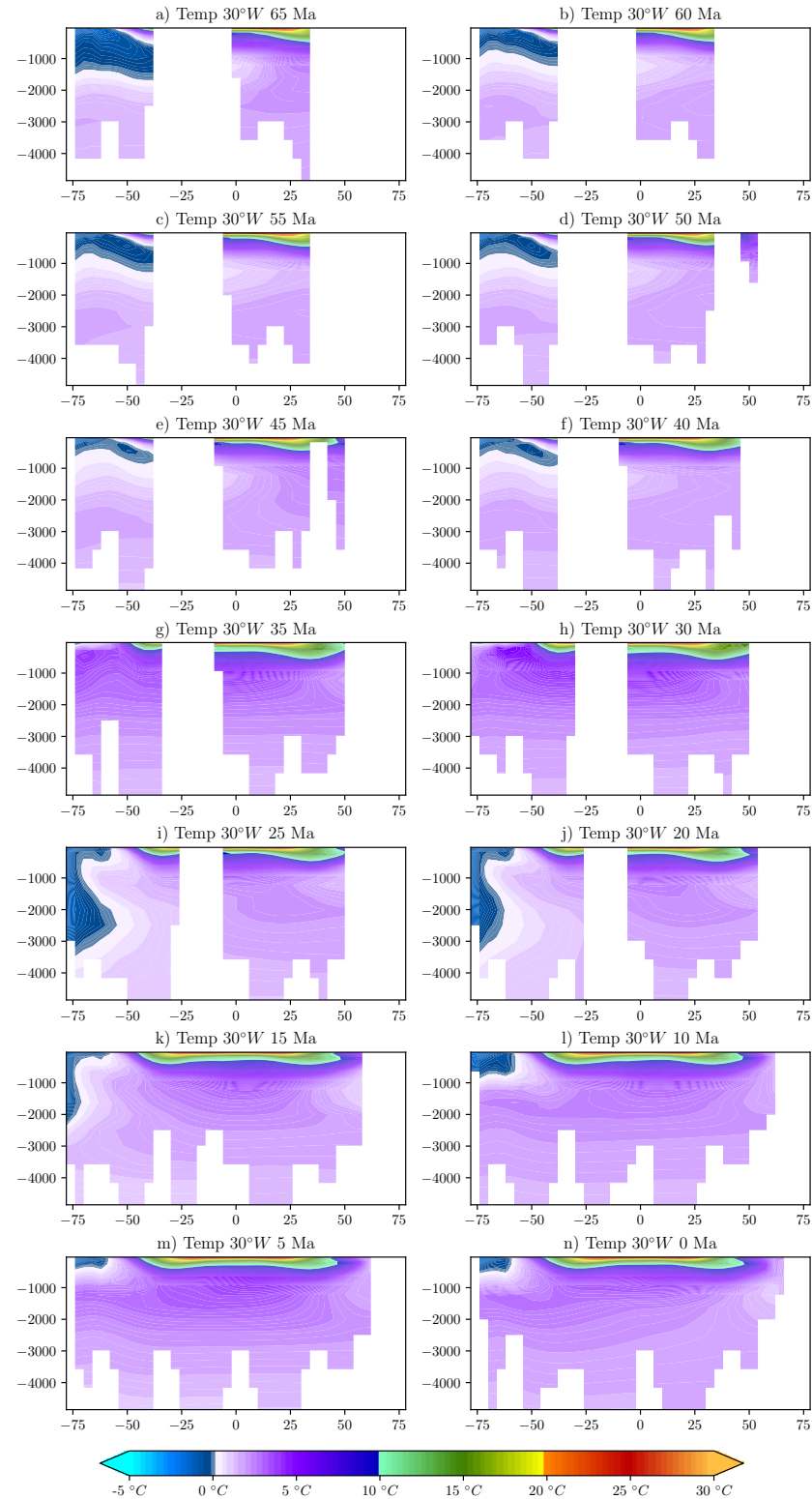


Figure 27: Latitude depth profile of the Temperature in the Pacific (178°W)

Figure 28: Latitude depth profile of the Temperature in the Atlantic ($178^{\circ}W$)

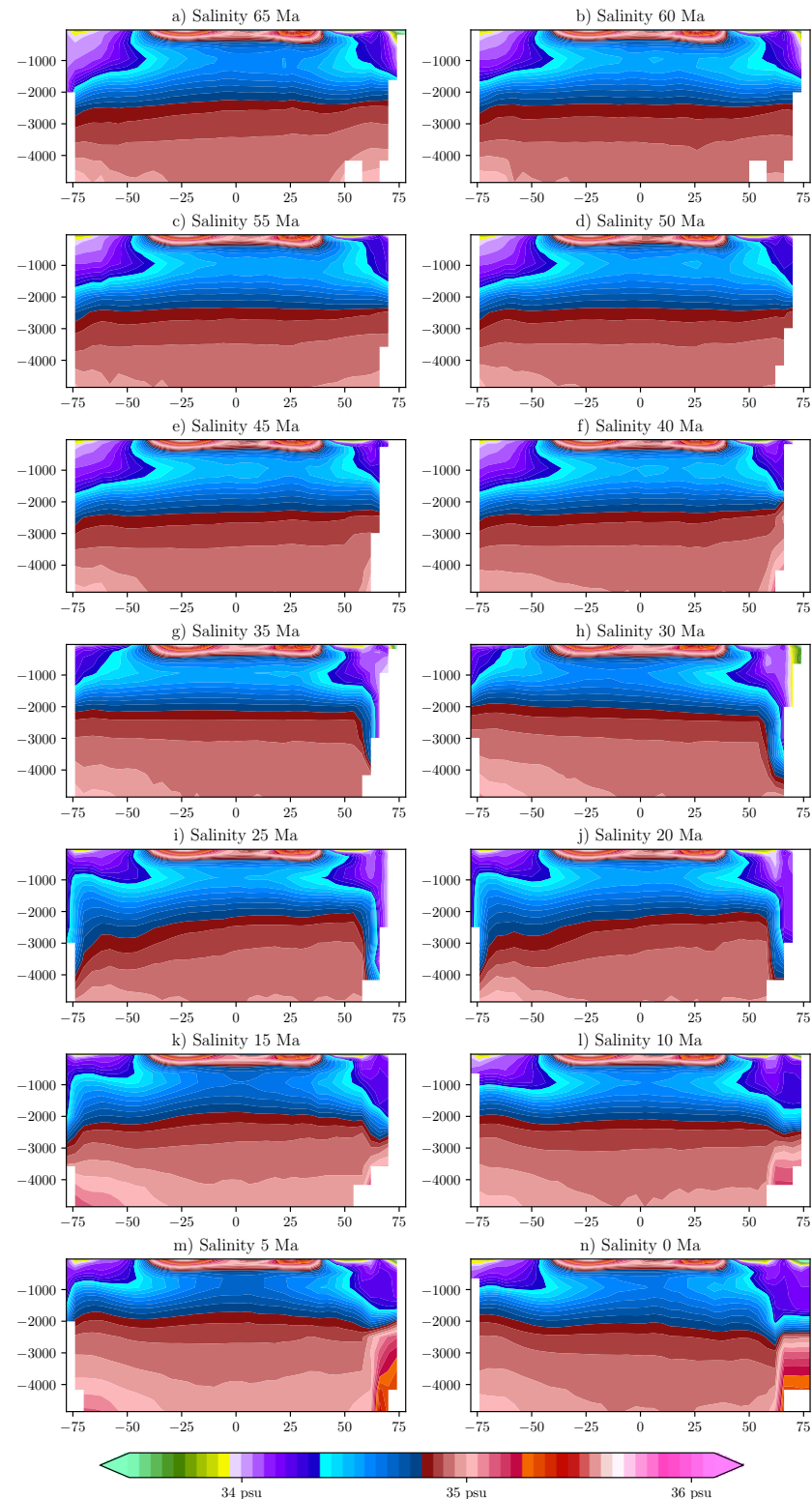


Figure 29: Latitude depth profile of the zonal mean Salinity

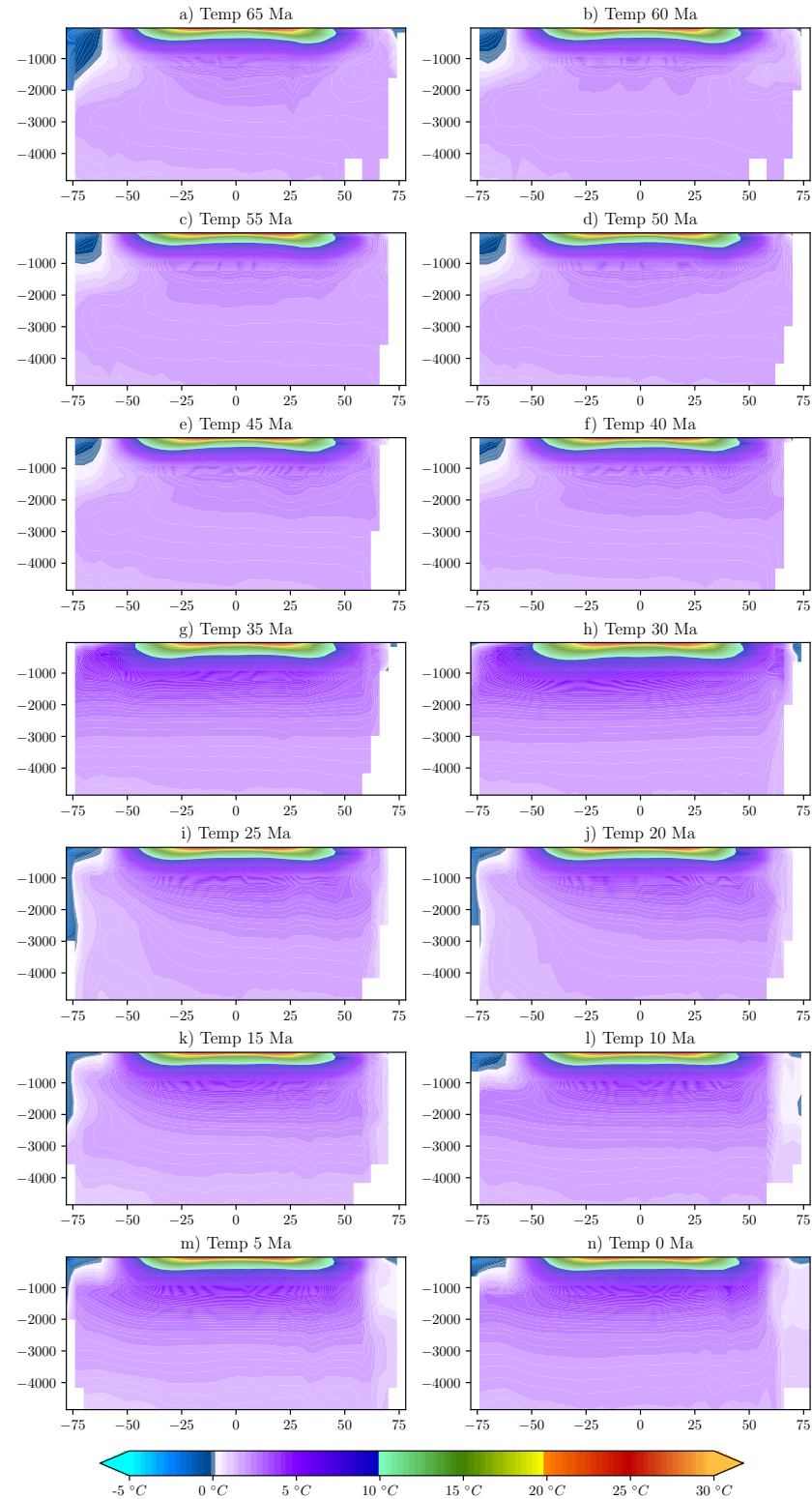


Figure 30: Latitude depth profile of the zonal mean temperature